High Energy Resolution Hard X-Ray and Gamma-Ray Imagers Using CdTe Diode Devices

Shin Watanabe, Shin-nosuke Ishikawa, Hiroyuki Aono, Shin'ichiro Takeda, Hirokazu Odaka, Motohide Kokubun, Tadayuki Takahashi, Kazuhiro Nakazawa, Hiroyasu Tajima, Mitsunobu Onishi, and Yoshikatsu Kuroda

***Abstract*—We developed CdTe double-sided strip detectors (DSDs or cross strip detectors) and evaluated their spectral and imaging performance for hard X-rays and gamma-rays. Though the double-sided strip configuration is suitable for imagers with a fine position resolution and a large detection area, CdTe diode DSDs with indium (In) anodes have yet to be realized due to the difficulty posed by the segmented In anodes. CdTe diode devices with aluminum (Al) anodes were recently established, followed by a CdTe device in which the Al anodes could be segmented into strips. We developed CdTe double-sided strip devices having Pt cathode strips and Al anode strips, and assembled prototype CdTe DSDs. These prototypes have a strip pitch of 400 μm. Signals from the strips are processed with analog ASICs (application specific integrated circuits). We have successfully performed gamma-ray imaging spectroscopy with a position resolution of 400 μm. Energy resolution of 1.8 keV (FWHM: full width at half maximum) was obtained at 59.54 keV. Moreover, the possibility of improved spectral performance by utilizing the energy information of both side strips was demonstrated. We designed and fabricated a new analog ASIC, VA32TA6, for the readout of semiconductor detectors, which is also suitable for DSDs. A new feature of the ASIC is its internal ADC function. We confirmed this function and good noise performance that reaches an equivalent noise charge of 110 e^- under the condition of 3–4 pF input capacitance.**

***Index Terms*—CdTe detectors, CZT detectors, gamma-ray detectors, imaging Spectrometers, strip detectors.**

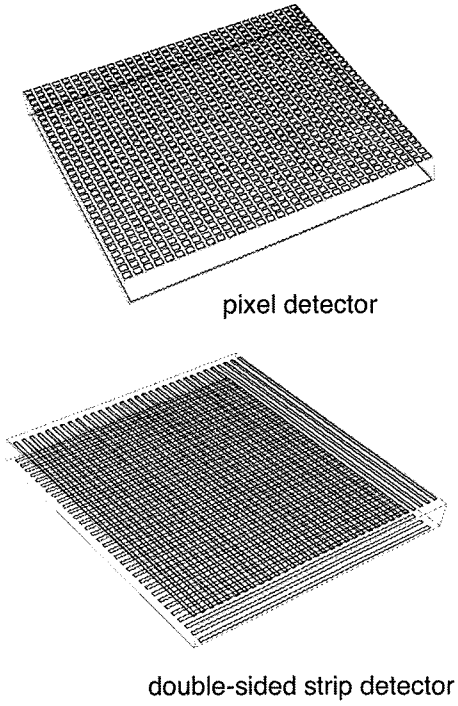

Fig. 1. Pixel detector and double-sided strip detector.

I. Introduction

HARD X-ray and gamma-ray imaging spectrometers with good spatial and energy resolutions are desired for medical, industrial and astrophysical applications. Cadmium telluride (CdTe) and cadmium zinc telluride (CZT) are very promising materials for hard X-ray and gamma-ray imaging spectrometers, given their high detection efficiency comparable to that of NaI scintillators and good energy resolution comparable to that of Ge detectors. Although both CdTe and CZT are vulnerable to energy resolution and peak detection efficiency being degraded due to their poor charge transport properties, several techniques have been developed to maintain good spectral performance [1], [2].

CdTe/CZT semiconductor detectors require segmented readout electrodes in order to obtain position information. For imagers having a fine position resolution, there are two types of detector configurations: pixel detectors and double-sided strip detectors (Fig. 1).

A pixel detector has a number of small pixel electrodes on one side. The signal from each pixel is processed with each charge-sensitive amplifier. Since the leakage current and the detector capacitance become very small, ideal spectral performance is consequently possible. However, an extremely large number of readout channels are needed for a fine position resolution and/or large detection area. Additionally, a two-dimensional readout ASIC is essential for fine pitch pixels [3]–[5].

Manuscript received June 30, 2008; revised September 12, 2008. Current version published June 17, 2009. This work was supported by KAKENHI(19740172).

S. Watanabe, S. Ishikawa, H. Aono, S. Takeda, H. Odaka, and T. Takahashi are with the Institute of Space and Astronautical Science, Japan Aerospace Exploration Agency, Sagamihara, Kanagawa, Japan, and also with the Department of Physics, University of Tokyo, Tokyo, Japan (e-mail: watanabe@astro.isas.jaxa.jp; ishikawa@astro.isas.jaxa.jp; aono@astro.isas.jaxa.jp; takeda@astro.isas.jaxa.jp; odaka@astro.isas.jaxa.jp; takahasi@astro.isas.jaxa.jp).

M. Kokubun is with the Institute of Space and Astronautical Science, Japan Aerospace Exploration Agency, Sagamihara, Kanagawa, Japan (e-mail: kokubun@astro.isas.jaxa.jp).

K. Nakazawa is with the Department of Physics, University of Tokyo, Tokyo, Japan (e-mail: nakazawa@amalthea.phys.s.u-tokyo.ac.jp).

H. Tajima is with the SLAC National Accelerator Laboratory, Menlo Park, CA 94025 USA (e-mail: htajima@slac.stanford.edu).

M. Onishi and Y. Kuroda are with Nagoya Guidance and Propulsion Systems Works, Mitsubishi Heavy Industry. Ltd., Komaki, Aichi, Japan (e-mail: mitsunobu_onishi@mhi.co.jp; yoshikatsu_kuroda@mhi.co.jp).

Digital Object Identifier 10.1109/TNS.2008.2008806

A double-sided strip detector (DSD or cross strip detector) realizes a fine position resolution and large detection area with a relatively small number of readout channels. The DSD has orthogonal strips implemented on both its sides. By reading out the signal from both side strips coincidentally, it is possible to obtain information on the position and energy of the X-ray/gamma-ray photons [6], [7]. The number of the readout channels is proportional to $2N$ (where N denotes the number of segments per coordinate) for DSDs, instead of N^2 for pixel detectors. Therefore, for a larger N (meaning a finer position resolution and/or larger area), the DSD has an advantage in terms of readout channels. Moreover, one-dimensional ASICs that are easier to implement and more common than two-dimensional ones are also applicable to DSDs.

Our development is aimed at hard X-ray imaging detectors for the ASTRO-H (NeXT) project that plans to launch Japan's 6th X-ray astronomy satellite in 2013. Among the major objectives is achieving high sensitivity observation with focusing and imaging capabilities in the 5–80 keV energy region. The ASTRO-H satellite will carry two hard X-ray telescopes that feature multilayer supermirrors assembled in grazing incident X-ray telescopes. Hard X-ray Imagers (the focal plane detectors of hard X-ray telescopes) require an energy resolution of ~1 keV (FWHM: full width at half maximum), energy coverage of 5–80 keV, a sub-mm (250–500 μm) position resolution, detection area of 2–3 cm, and timing resolution of $\sim$ 1 μs for high sensitivity observation. To achieve these goals, we have developed CdTe diode DSDs as a primary choice for Hard X-ray Imagers. In this paper, we describe our development of CdTe DSDs, and report the results of the CdTe DSD prototypes. We also report on our newly developed ASIC (VA32TA6) for semiconductor detector readout.

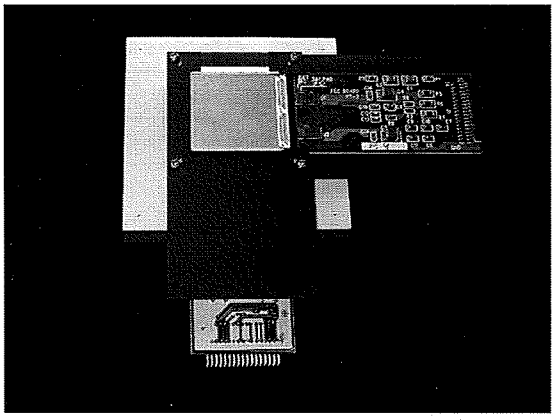

(a)

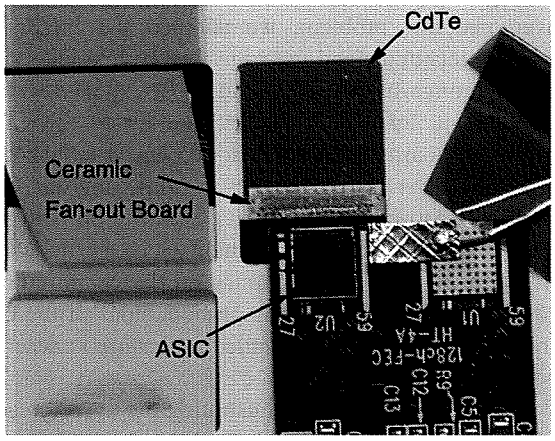

(b)

Fig. 2. Prototypes of the CdTe DSDs. (a): The 2.6 cm CdTe DSD. It is 2.6 cm × 2.6 cm in size and, 500 μm thick. The strip pitch is 400 μm. On each side 64 strips are formed, and two VA32TAs are used for readout on each side. (b): The 1.3 cm CdTe DSD. It is 1.3 cm × 1.3 cm in size, and 500 μm thick. The strip pitch is 400 μm. On each side 32 strips are formed, and one VA64TA2 is used for readout on each side.

II. Prototypes of CdTe DSDs

A. CdTe Diode Device With Double-Sided Strips

Thin CdTe diode devices that utilize indium (In) as the anode electrodes on p-type CdTe wafers manufactured by ACRORAD (Japan) and platinum (Pt) as the cathodes have been established and offer good spectral performance [1]. A high Schottky barrier formed on the In/p-CdTe interface enables use of the detector as a diode. Using this type of detector with a thickness of 0.5 mm at applied bias voltages as high as 1 kV makes it possible to overcome the poor charge transport properties of CdTe. However, double-sided strip detectors with In anodes cannot be realized since it is difficult to segment the In electrode into strips.

Aluminum (Al) has recently been found to be a good alternative electrode material to In [8], [9]. In addition to low leakage currents and high energy resolutions comparable to those of In/CdTe/Pt detectors, Al/CdTe/Pt detectors also offer the advantage of allowing Al anodes to be divided into pixels or strips. CdTe diode detectors with segmented Al anodes have been established by constructing and testing Al-pad/CdTe/Pt or Al-pixel/CdTe/Pt type detectors. Good spectral performance ($\Delta E \sim$ 1 keV (FWHM) at 60 keV) has been achieved [10], [11].

By adopting segmented Al anodes and Pt cathodes, we can obtain a CdTe diode double-sided strip device. For the prototype detectors, we fabricated two types of the CdTe devices: the 2.6 cm CdTe device and 1.3 cm CdTe device. The 2.6 cm CdTe device is 2.6 cm × 2.6 cm in size, and 500 μm thick. On each side 64 strips are formed, with a strip pitch of 400 μm. Moreover, 350 μm strip electrodes and 50 μm gaps are alternately formed. The 1.3 cm CdTe device is 1.3 cm × 1.3 cm in size, and 500 μm thick. On each side 32 strips are formed. The strip pitch and electrode configuration are the same as those of the 2.6 cm CdTe DSD. Both devices have guard-ring electrodes on both sides to reduce leakage current of the strips.

B. Configurations of Prototypes

We used the CdTe double-sided strip devices described above to assemble two types of prototype CdTe DSDs: the 2.6 cm CdTe DSD and the 1.3 cm CdTe DSD. Fig. 2 shows the prototype detectors. We employed VA32TAs [12] and VA64TA2s [13] that we jointly developed with GM-IDEAS to read out the 2.6 cm and the 1.3 cm CdTe DSDs, respectively.

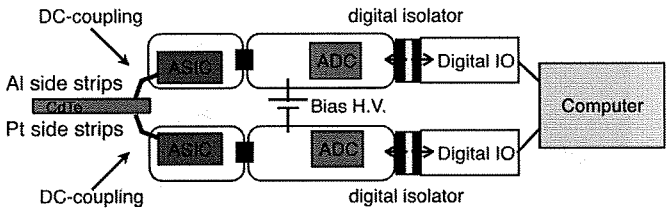

Fig. 3. Readout system of the CdTe DSDs.

Given the soft and fragile characteristics of CdTe material, we have yet to establish a reliable technique of wire-bonding on the CdTe surface. Therefore, it is difficult to interconnect the CdTe strip electrodes and the readout ASIC input pads by using wire-bonding as applied to Si DSDs [14], [15].

To overcome this problem, we adopted the In/Au stud bump bonding technique and used the Al_2O_3 ceramic fan-out board with through-holes. First, the CdTe strip electrodes are connected via In/Au stud bump bonding to the Al_2O_3 ceramic fan-out board that we developed and established for CdTe-Pixel/Pad detectors [16]. This ceramic fan-out board has through-holes to interconnect the electrodes on both sides of the fan-out board. Then, wire-bonding can be done from the ASIC input pads to the electrodes on the ceramic board. We have connected readout ASICs on both sides of the CdTe DSDs in this manner. A more detailed procedure is described in elsewhere [17].

Fig. 3 shows a block diagram illustrating the overall readout system. This system is virtually the same as the scheme implemented for the readout of Si DSDs [14], [15]. The readout ASICs and strip electrodes are connected with DC-coupling for both sides. The detector bias voltage is supplied by applying a high voltage between local grounds of the Al anodes and Pt cathodes.

C. Imaging and Spectral Performance

In order to demonstrate the imaging capability of the test devices, we took shadow images of metal objects with various gamma rays from radioisotopes such as ^{241}Am, ^{133}Ba and ^{57}Co. Fig. 4 shows the shadow images obtained with the 2.6 cm CdTe DSD and the target. The hole of a 2-mm nut and solder 0.6 mm diameter can be clearly seen. It can also be seen that a thin washer becomes transparent as the energy of gamma rays becomes higher. However, the energy resolution obtained with the 2.6 cm CdTe DSD did not match that obtained with pad-type Al anode detectors. FWHM energy resolutions of 2.6 keV and 6.2 keV at 59.54 keV were obtained for the spectra from Pt strips and Al strips, respectively, under 500 V of bias voltage and temperature of $-20°$C.

For a detailed study of spectral performance, we tested a 1.3 cm CdTe DSD. The smaller capacitance and lower leakage current afforded by smaller detector size should lead us to better noise performance. The spectral performance of VA64TA2 for negative signals from the Al strips has also been improved compared with VA32TA used in the 2.6 cm CdTe DSD.

Fig. 5 show the spectra obtained with the 1.3 cm CdTe DSD. Under operating conditions of $-20°$C temperature and 500 V of applied bias voltage, the total leakage current from all strips and guard-rings was 5 nA. The trigger energy threshold can be set to about 10 keV. An energy resolution of 1.8 keV (FWHM) at 59.54 keV was obtained for both the Pt and Al sides. The spectral performance for the Al and Pt sides was confirmed as being equivalent in the CdTe DSDs.

By collectively using the energy information on both sides, improved spectral performance could be expected if each noise component was independent. We created a spectrum by filling the average of the both sides' energy information, as shown in Fig. 6. This spectrum shows improved energy resolution. Thus, an energy resolution of 1.4 keV (FWHM) was successfully obtained.

For imagers, uniform spectral performance in each detector is important. In the double-sided strip configuration, we can examine a kind of uniformity by sorting the events of one strip based on the position information obtained from the other side's strips. Since only one channel of the ASIC is used for the readout, we can obtain the position dependence without the effect of readout variation. Fig. 7 shows a ^{241}Am gamma-ray spectrum from one strip on the Al side. The Y axis corresponds to the hit strip on the Pt side. It can be seen that the spectrum is constant with the position. The peak position and energy resolution for 59.54 keV gamma rays were stable within 0.2% and 12%, respectively.

III. Brand New Readout ASIC, VA32TA6

We have been developing readout ASICs for our applications in collaboration with GM-IDEAS. Based on past developments, we designed and fabricated a new readout ASIC, VA32TA6. Fig. 8 shows a photograph of VA32TA6 and a schematic diagram of the ASIC. VA32TA6 is fabricated using AMS 0.35 μm technology with an epitaxial layer. The die is 5.0 mm $\times$ 7.8 mm in size and 725 μm thick. The front-end part of VA32TA6 is based on VA64TA1 [13]. It has 32 channels of circuits, including a charge-sensitive amplifier, slow CR-RC shaper and sample/hold (VA section), and fast CR-RC shaper and discriminator chain (TA section). The shaping time of the slow shaper is variable from 2 to 4 μs: that of the fast shaper is 600 ns. A detailed description of this VA-TA architecture is given in other [12], [14]. The measured power consumption on average was 16.5 mW per chip, corresponding to 0.5 mW per channel by considering a simple division of channel numbers.

The main new feature of VA32TA6 is the inclusion of on-chip ADC circuitry. VA32TA6 implements a Wilkinson-type ADC that digitizes the 32 sampled pulse heights of the slow shapers in parallel. The ramp speed is adjustable via the internal DAC. The ADC clock's maximum speed is 10 MHz. Each channel has a 10-bit digital counter. The maximum dead time due to AD conversion is $\sim$ 100 μs under the 10 MHz ADC clock. The ADC circuitry is equipped with a global Common Mode Detection Unit. This unit latches the ADC counter value when a certain number of channel discriminators have fired. For VA32TA6, the threshold of the Common Mode Detection Unit has one default setting (16 channels). The common mode value is stored in a separate counter and output as part of the data stream.

To evaluate the functions and performance of the ASIC, we constructed CdTe pad detectors for connection to VA32TA6. Each pad is 1.35 mm $\times$ 1.35 mm in size. A total of 32 pads

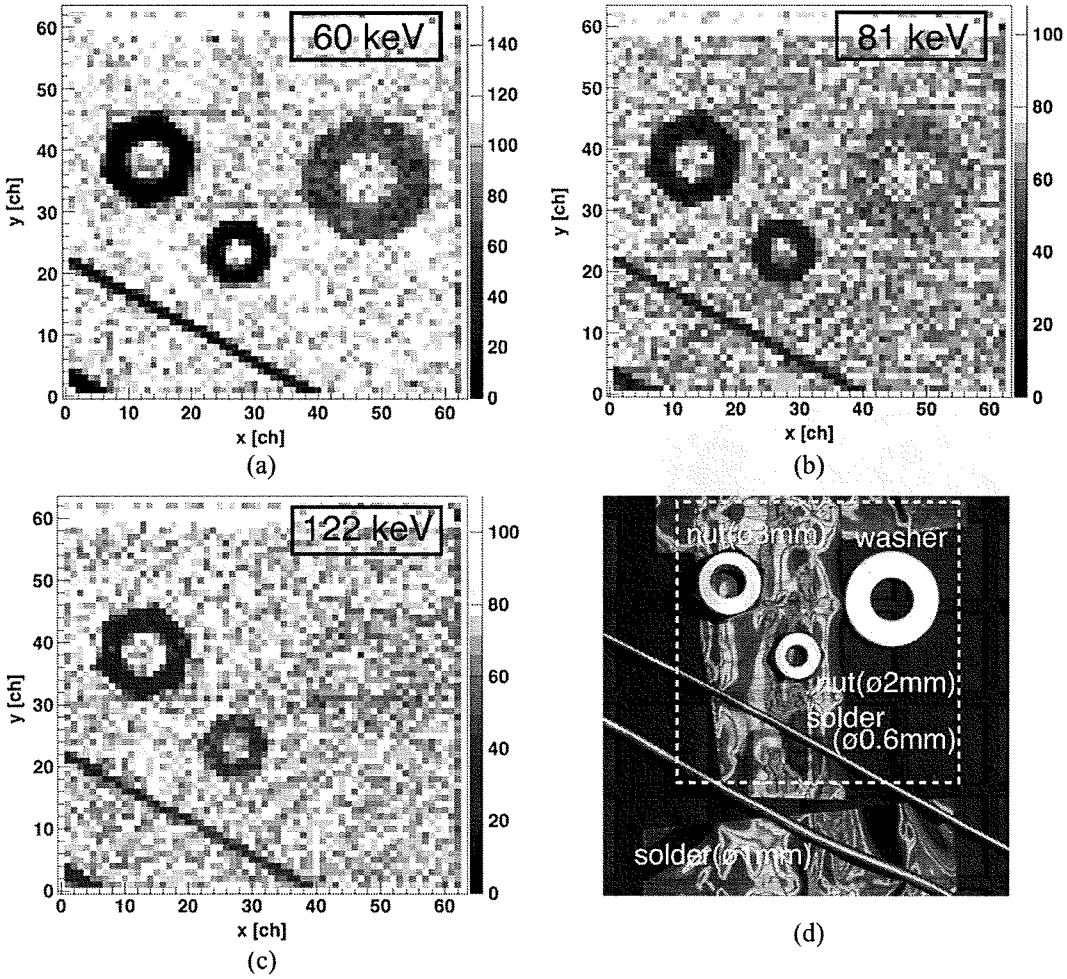

Fig. 4. Shadow images obtained with the 2.6 cm CdTe DSD and a photograph of the target. The energies of the gamma rays are 60 keV (^{241}Am), 81 keV (^{133}Ba) and 122 keV (^{57}Co). The pixel size in the images corresponds to a strip pitch of 400 μm.

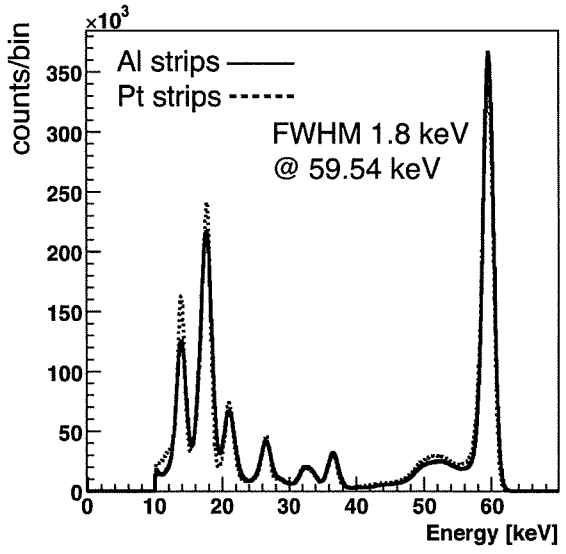

Fig. 5. ^{241}Am spectra obtained with the 1.3 cm CdTe DSD. The solid and dotted lines indicate spectra from the Al and Pt strips, respectively. A bias voltage of 500 V was applied at operating temperature of -20°C. An energy resolution of 1.8 keV(FWHM) at 59.54 keV was obtained for both sides.

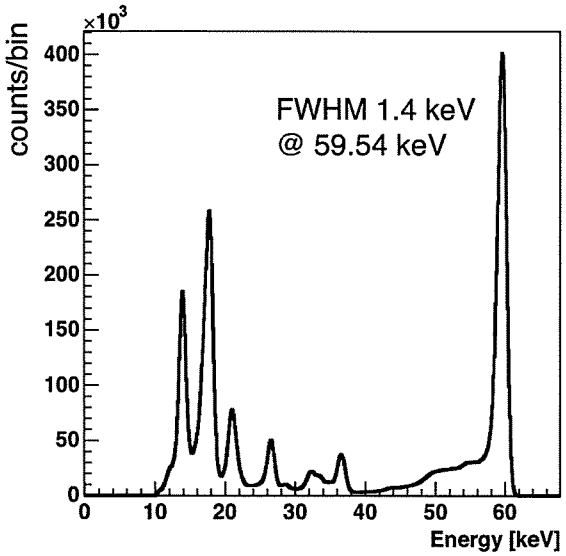

Fig. 6. ^{241}Am spectra obtained with the 1.3 cm CdTe DSD. The average of the both sides' energy information was used. The energy resolution was improved to 1.4 keV(FWHM) at 59.54 keV.

(in $8 \times 8 = 64$ pads) are connected to the ASIC. The pad capacitance is expected to be 3–4 pF per channel. We used two types of CdTe pad detectors. One is an In/CdTe/Pt-pad type detector [18], in which VA32TA6 is connected to Pt cathode pads, for processing positive charge signals. The other is an

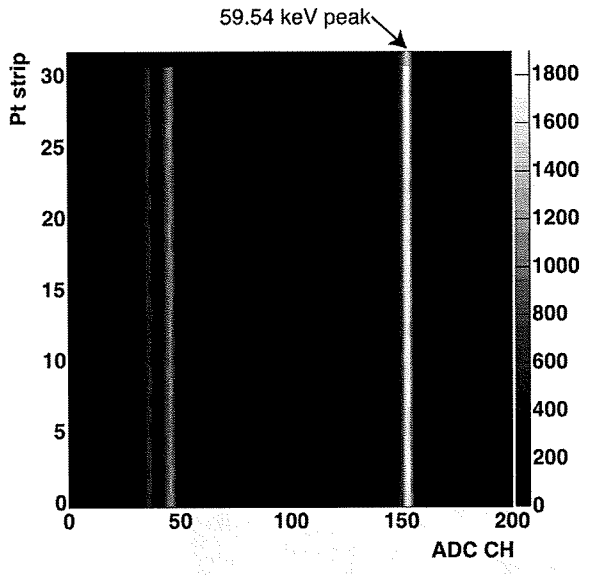

Fig. 7. ^{241}Am spectra obtained with one Al strip of the 1.3 cm CdTe DSD. The X and Y axes correspond to the Al strip's pulse height in the ADC channel and the hit strip on the Pt side, respectively.

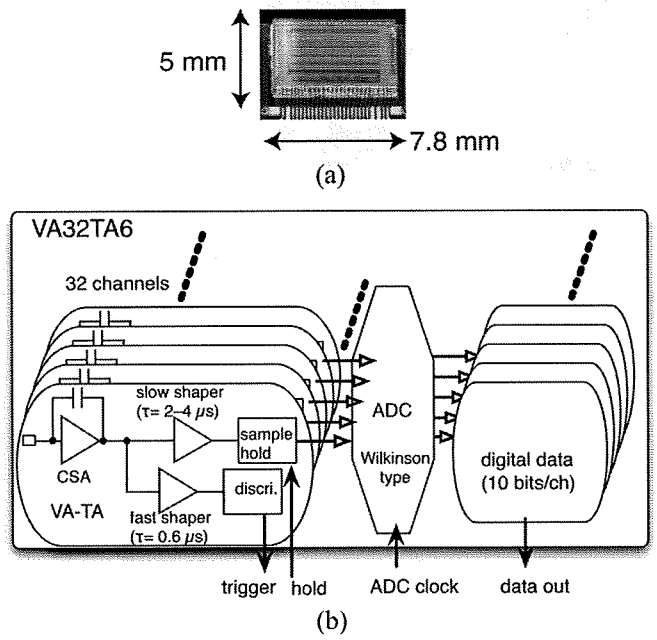

Fig. 8. Photograph of VA32TA6 and a schematic diagram.

Al-pad/CdTe/Pt type detector [10]. The ASIC in this detector is connected to Al anode pads for processing negative charge signals.

By applying a detector bias voltage and irradiating the detector with X-rays/gamma rays emitted by a radioisotope, we have successfully made VA32TA6s work and have obtained digital pulse height data. The ADC circuitry works properly with clock speed up to 10 MHz. Fig. 9 shows the obtained spectra from the CdTe pad detectors. These spectra are obtained from a single channel of the pad detectors. The pedestal level is corrected, and the common mode is subtracted by using the data from the Common Mode Detection Unit. An energy resolution

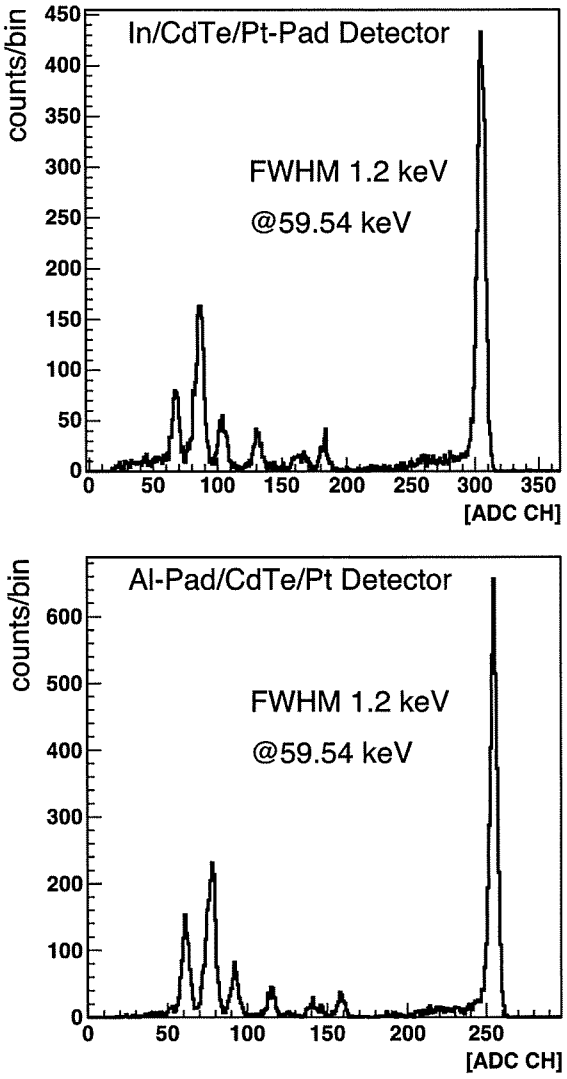

Fig. 9. ^{241}Am gamma-ray spectra obtained with CdTe pad detectors using VA32TA6. At an operating temperature of −20°C, bias voltages of 600 V and 400 V were applied for the In/CdTe/Pt-pad detector and Al-pad/CdTe/Pt detector, respectively. The pedestal level was corrected, and the common mode was subtracted by using the data from the Common Mode Detection Unit. An energy resolution of 1.2 keV (FWHM) at 59.54 keV was achieved.

of 1.2 keV (FWHM) at 59.54 keV was achieved for both pad detectors. This energy resolution in CdTe corresponds to 110 e^- in ENC (equivalent noise charge). This spectral performance is comparable with that of VA64TA1 [13].

For our astrophysical application, it is important to achieve as low an energy threshold as possible. Fig. 10 demonstrates the low energy threshold. This is an X-ray spectrum from ^{55}Fe obtained with one channel of the Al-pad/CdTe/Pt detector. The Mn K X-ray line combining a 5.9 keV Kα and a 6.4 keV Kβ was detected and clearly resolved. The energy threshold can be set as low as 4 keV, which satisfies the energy coverage goal of Hard X-ray Imagers used in the ASTRO-H (NeXT) project.

IV. Conclusion

We developed CdTe diode double-sided strip detectors that have Al anode and Pt cathode strips. Two types of prototypes were assembled and we evaluated their imaging capability and

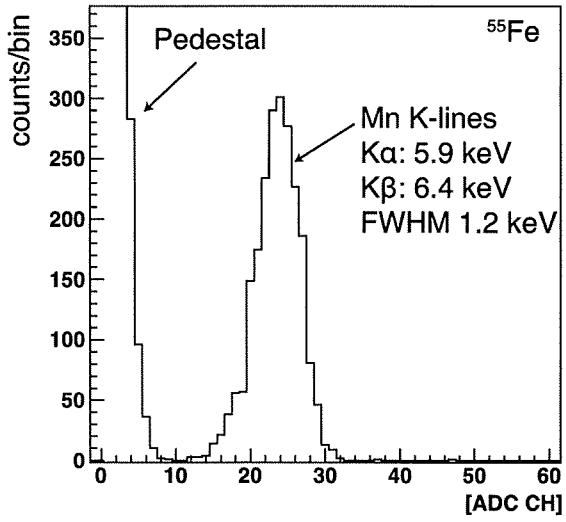

Fig. 10. ^{55}Fe X-ray spectrum obtained with the Al-pad/CdTe/Pt detector using VA32TA6. At operating temperature of −20°C, 400 V of bias voltage was applied. The pedestal level was corrected, and the common mode was subtracted by using the data from the Common Mode Detection Unit.

spectral performance. Gamma-ray imaging spectroscopy with a position resolution of 400 μm was demonstrated by using the 2.6 cm CdTe DSD. The energy resolution of 1.8 keV (FWHM) at 59.54 keV was obtained with the 1.3 cm CdTe DSD.

For semiconductor detector readout, we have developed a new analog ASIC, VA32TA6, characterized by a main new feature of including an on-chip ADC. By constructing CdTe pad detectors, we tested the functions and performance of VA32TA6. The ADC worked properly and good noise performance was obtained.

We are developing the next version of the CdTe DSD, that will use VA32TA6s as the readout ASICs. By using VA32TA6s, the readout system may be simplified, because it is possible to control the ASICs and read data by only using digital signals. Such a new configuration would offer improvements in performance as required for the the ASTRO-H (NeXT) Hard X-ray Imager and future X-ray/gamma-ray telescopes.

REFERENCES

[1] T. Takahashi and S. Watanabe, "Recent progress in CdTe and CdZnTe detector," *IEEE Trans. Nucl. Sci.*, vol. 48, no. 4, pp. 950–959, 2001.

[2] O. Limousin, "New trends in CdTe and CdZnTe detectors for X- and gamma-ray applications," *Nucl. Instr. Meth.*, vol. A 504, pp. 24–37, 2003.

[3] F. A. Harrison, S. E. Boggs, A. E. Bolotnikov, C. M. H. Chen, W. R. Cook, and S. M. Schindler, "Development of CdZnTe pixel detectors for astrophysical applications," in *Proc. SPIE*, 2000, vol. 4141, pp. 137–143.

[4] A. E. Bolotnikov, W. R. Cook, S. E. Boggs, F. A. Harrison, and S. M. Schindler, "Development of high spectral resolution CdZnTe pixel detectors for astronomical hard x-ray telescopes," *Nucl. Instr. Meth.*, vol. A 458, pp. 585–592, 2001.

[5] K. Oonuki, H. Inoue, K. Nakazawa, T. Mitani, T. Tanaka, T. Takahashi, C. M. H. Chen, W. R. Cook, and F. A. Harrison, "Development of uniform CdTe pixel detectors based on caltech ASIC," in *Proc. SPIE*, 2004, vol. 5501, pp. 218–228.

[6] K. R. Slavis *et al.*, "High altitude balloon flight of CdZnTe detectors for high energy x-ray astronomy," in *Proc. SPIE*, 1998, vol. 3445, pp. 169–183.

[7] E. Kalemci and J. L. Matteson, "Investigation of charge sharing among electrode strips for a CdZnTe detector," *Nucl. Instr. Meth.*, vol. A 478, pp. 527–537, 2002.

[8] H. Toyama, A. Nishihira, M. Yamazato, A. Higa, T. Maehama, R. Ohno, and M. Toguchi, "Formation of Aluminum Schottky Contact on Plasma-Treated Cadmium Telluride Surface," *J.J. Appl. Phys.*, vol. 43, no. 9A, pp. 6371–6375, 2004.

[9] H. Toyama, M. Yamazato, A. Higa, T. Maehama, R. Ohno, and M. Toguchi, "Effect of He plasma treatment on the rectification properties of Al/CdTe Schottky contacts," *J.J. Appl. Phys.*, vol. 44, no. 9A, pp. 6742–6746, 2005.

[10] S. Watanabe, S. Ishikawa, S. Takeda, H. Odaka, T. Tanaka, T. Takahashi, K. Nakazawa, M. Yamazato, A. Higa, and S. Kaneku, "New CdTe pixel gamma-ray detector with pixelated Al Schottky anodes," *J.J. Appl. Phys.*, vol. 46, no. 9A, pp. 6043–6045, 2007.

[11] A. Meuris, O. Limousin, F. Lugiez, O. Gevin, F. Pinsard, I. Le Mer, E. Delagnes, M. C. Vassal, F. Soufflet, and R. Bocage, "Caliste 64, an innovative CdTe hard x-ray micro-camera," *IEEE Trans. Nucl. Sci.*, vol. 55, pp. 778–784, 2008.

[12] H. Tajima, T. Nakamoto, T. Tanaka, S. Uno, T. Mitani, E. do Couto e Silva, Y. Fukazawa, T. Kamae, G. Madejski, D. Marlow, K. Nakazawa, M. Nomachi, Y. Okada, and T. Takahashi, "Performance of a low noise front-end ASIC for Si/CdTe detectors in Compton Gamma-ray telescope," *IEEE Trans. Nucl. Sci.*, vol. 51, pp. 842–847, 2004.

[13] T. Tanaka, S. Watanabe, S. Takeda, K. Oonuki, T. Mitani, K. Nakazawa, T. Takashima, T. Takahashi, H. Tajima, N. Sawamoto, Y. Fukazawa, and M. Nomachi, "Recent results from a Si/CdTe semiconductor Compton telescope," *Nucl. Instr. Meth.*, vol. A 568, pp. 375–381, 2006.

[14] H. Tajima, T. Kamae, S. Uno, T. Nakamoto, Y. Fukazawa, T. Mitani, T. Takahashi, K. Nakazawa, Y. Okada, and M. Nomachi, "Low noise double-sided silicon strip detector for multiple-Compton gamma-ray telescope," in *Proc. SPIE*, 2003, vol. 4851, pp. 875–884.

[15] S. Takeda, S. Watanabe, T. Tanaka, K. Nakazawa, T. Takahashi, Y. Fukazawa, H. Yasuda, H. Tajima, Y. Kuroda, M. Onishi, and K. Genba, "Development of double-sided silicon strip detectors (DSSD) for a Compton telescope," *Nucl. Instr. Meth.*, vol. A 579, pp. 859–865, 2007.

[16] T. Takahashi *et al.*, "High Resolution CdTe Detector and Applications to Image Devices," *IEEE Trans. Nucl. Sci.*, vol. 48, pp. 287–291, 2001.

[17] T. Takahashi, S. Ishikawa, S. Watanabe, K. Nakazawa, Y. Kuroda, and M. Onishi, "A CdTe diode double-sided strip detector," *Nucl. Instr. Meth.*, 2008, A, submitted for publication.

[18] S. Watanabe, S. Takeda, S. Ishikawa, H. Odaka, M. Ushio, T. Tanaka, K. Nakazawa, T. Takahashi, H. Tajima, Y. Fukazawa, Y. Kuroda, and M. Onishi, "Development of Semiconductor Imaging Detectors for a Si/CdTe Compton Camera," *Nucl. Instr. Meth.*, vol. A 579, pp. 871–877, 2007.

Experimental Results of the Gamma-Ray Imaging Capability With a Si/CdTe Semiconductor Compton Camera

Shin'ichiro Takeda, Hiroyuki Aono, Sho Okuyama, Shin-nosuke Ishikawa, Hirokazu Odaka, Shin Watanabe, Motohide Kokubun, Tadayuki Takahashi, Kazuhiro Nakazawa, Hiroyasu TajimaHiro, and Naoki Kawachi

***Abstract*—A semiconductor Compton camera that combines silicon (Si) and Cadmium Telluride (CdTe) detectors was developed, and its imaging capability was examined with various kinds of gamma-ray targets such as a point source, arranged point sources and an extended source. The camera consists of one double-sided Si strip detector and four layers of CdTe pad detectors, and was designed to minimize the distance between a scatterer and the target. This is because the spatial resolution with Compton imaging improves as the target approaches the scatterer. This new camera realizes a minimum distance of 25 mm. By placing the target at a distance of 30 mm from the detector, resolving power better than 3 mm was demonstrated experimentally for a 364 keV (^{131}I) gamma-ray. Positional determination with accuracy of 1 mm was also demonstrated. As a deconvolution method, we selected the iteration algorithm (called List-Mode Expectation-Maximizing Maximum Likelihood), and applied it to several kinds of experimental data. The Compton back projection images of the arranged point sources and an extended object were successfully deconvolved.**

***Index Terms*—CdTe detector, Compton camera, gamma-ray imaging, silicon strip detector.**

I. Introduction

COMPTON imaging is an attractive technology used in gamma-ray detection for various applications. In high energy astrophysics, high-sensitivity gamma-ray observation is required for studying nucleosynthesis and particle acceleration, the phenomena of which are widely observed throughout the vast universe. The technology is also applicable to nuclear medical imaging and/or non-destructive inspection [1], [2], since it can directly locate the position of gamma-ray signals with a wide field of view, as well as a wide energy band.

We have developed a Compton camera—the Si/CdTe Compton camera [3]–[6]—based on the combination of Silicon (Si) and Cadmium Telluride (CdTe) semiconductor detectors. It consists of many layers of thin Si and CdTe position-sensitive detectors. The design leads to a high-angular resolution thanks to the high-energy and position resolution of these semiconductor detectors, including dedicated low-noise analog ASICs. Si is a suitable scatterer material, given its smaller Doppler broadening effect than that of any other semiconductor devices [7]. This effect is caused by the non-zero momenta of electrons, and imposes a theoretical limit on angular resolution. CdTe works very nicely as an absorber thanks to its large atomic numbers (48, 52) and high density (5.8 g/cm^3).

In our previous work, we developed a prototype Compton camera that was primarily designed for future balloon-borne astrophysics experiments [8], and verified its performance. The Compton reconstruction was successfully performed and the gamma-ray images of point sources were obtained from 662 keV down to 59.5 keV. The typical resolution of scattering angle (the Angular Resolution Measure or ARM) was 3.5° Full-Width-at-Half-Maximum (FWHM) and 2.5° (FWHM) at 356 keV and 511 keV, respectively.

A Compton camera with an angular resolution of a few degrees is an attractive detector applicable not only to astrophysics, but also to nuclear medical imaging. Such applications require spatial resolution at the mm level. In this paper, we report the experimental results of Compton imaging using a new detector designed for high spatial resolution in short-distance imaging. Fig. 1 shows a photo of the detector system. Section II describes our approach to obtaining high spatial resolution. Section III describes the key detectors mounted on the Compton camera and the camera's design. Section IV describes the procedure of Compton imaging, and Section V summarizes the imaging results.

II. Design Approach to High Spatial Resolution

In order to achieve the high spatial resolution of a short-distance target by using Compton imaging, designing the arrangement of detectors requires special care. Fig. 2 shows the schematic of a Compton camera consisting of two scatterers and one absorber. A gamma-ray photon emitted from a target is detected through two major scenarios: (a) scattered in the 1st scatterer or (b) in the 2nd scatterer, and then absorbed in the absorber

Manuscript received July 09, 2008; revised November 16, 2008. Current version published June 10, 2009. This work was supported in part by Gumma University's Faculty of Medicine and in part by the Japan Atomic Energy Agency under grant JSPS COE (biomedical research using accelerator technology).

S. Takeda, H. Aono, S. Ishikawa, H. Odaka, S. Watanabe, M. Kokubun and T. Takahashi are members of the Institute of Space and Astronautical Science, Japan Aerospace Exploration Agency, Kanagawa 229-8510, Japan, and also the Department of Physics, University of Tokyo, Tokyo 113-0033, Japan (e-mail: takeda@astro.isas.jaxa.jp; aono@astro.isas.jaxa.jp; ishikawa@astro.isas.jaxa.jp; odaka@astro.isas.jaxa.jp; watanabe@astro.isas.jaxa.jp; kokubun@astro.isas.jaxa.jp; takahasi@astro.isas.jaxa.jp).

S. Okuyama and K. Nakazawa are with the Department of Physics, University of Tokyo, Tokyo 113-0033, Japan (e-mail: okuyama@amalthea.phys.s.u-tokyo.ac.jp; nakazawa@amalthea.phys.s.u-tokyo.ac.jp).

H. Tajima is with the Stanford Linear Accelerator Center, Menlo Park, CA 94025 USA (e-mail: htajima@slac.stanford.edu).

N. Kawachi is with the Quantum Beam Science Directorate, Japan Atomic Energy Agency, Gunma 370-1292, Japan (e-mail: kawachi.naoki@jaea.go.jp).

Color versions of one or more of the figures in this paper are available online at http://ieeexplore.ieee.org.

Digital Object Identifier 10.1109/TNS.2008.2012059

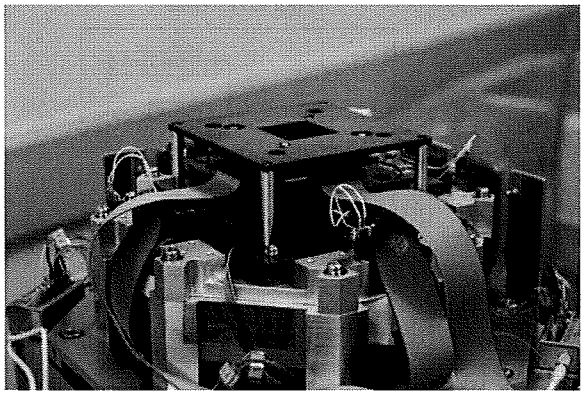

Fig. 1. Photograph of the Compton camera.

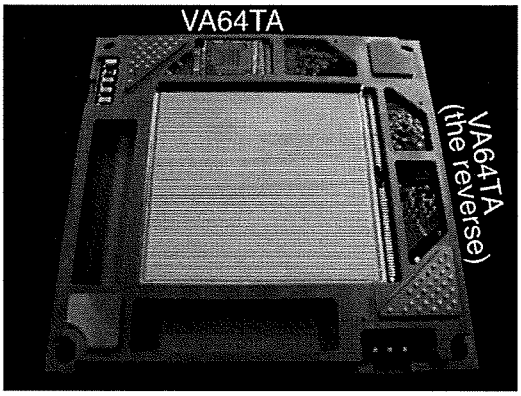

Fig. 3. Photograph of a DSSD board.

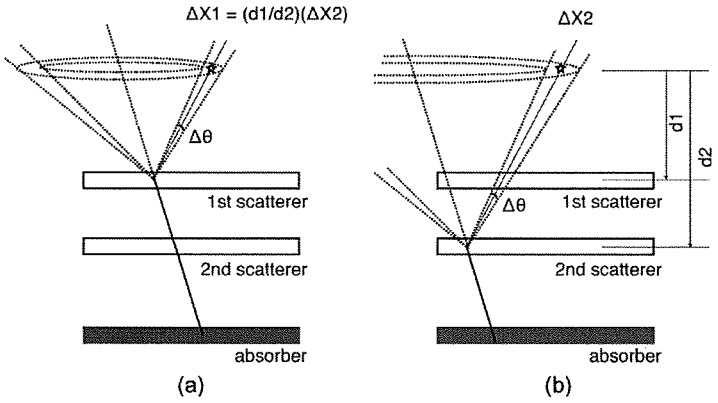

Fig. 2. Schematic of a Compton camera consisting of two scatterers and one absorber. Case (a) has a factor of (d1/d2) better spatial resolution, as derived from the angular resolution multiplied by the distance.

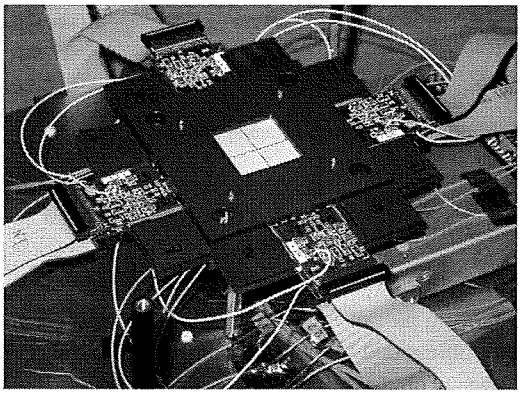

Fig. 4. Photograph of a 4-layer stacked CdTe module.

detector. The direction of incident photons is obtained as a cone in the sky (Compton cone) based on information about the interaction positions and related energy deposits in both the scatterer and absorber. By simply assuming that cases (a) and (b) have the same angular resolution, case (a) has a factor of (d1/d2) better spatial resolution, as derived from the angular resolution multiplied by the distance. Generally speaking, the spatial resolution in Compton imaging gradually deteriorates as the distance increases between the target and scatterer.

In our previous Compton camera [8], we used a Si scatterer consisting of four layers of a double-sided silicon strip detector (DSSD described in Section III-A) in order to improve detection efficiency [8], [9]. For astrophysical imaging, only the angular resolution and detection efficiency are essential since the targets are located virtually indefinitely in the far distance. Conversely, in a short-distance application, the 2nd to 4th layer of the scatterer degrades the spatial resolution, given the increasing distance to the target. Therefore, we employed one DSSD layer for the scatterer in the Compton camera described in this paper. It is also important to minimize the distance between 1st scatterer and a target. When considering the few degrees of angular resolution, the interval must be limited within a few tens of mm to obtain mm-scale spatial resolution. In our case, a minimum distance of 25 mm to a target was achieved.

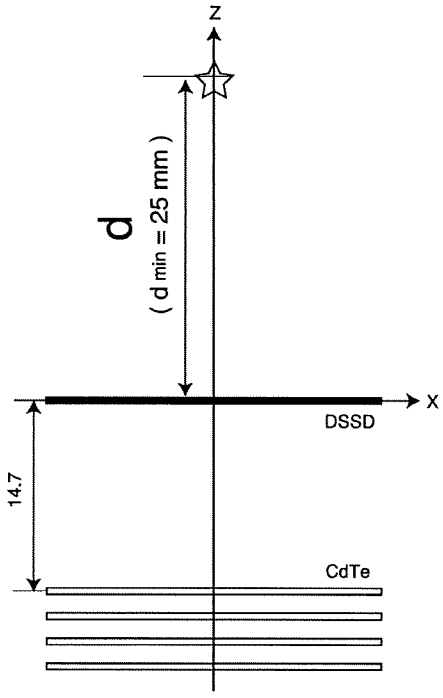

Fig. 5. Cross-sectional view of the Compton camera.

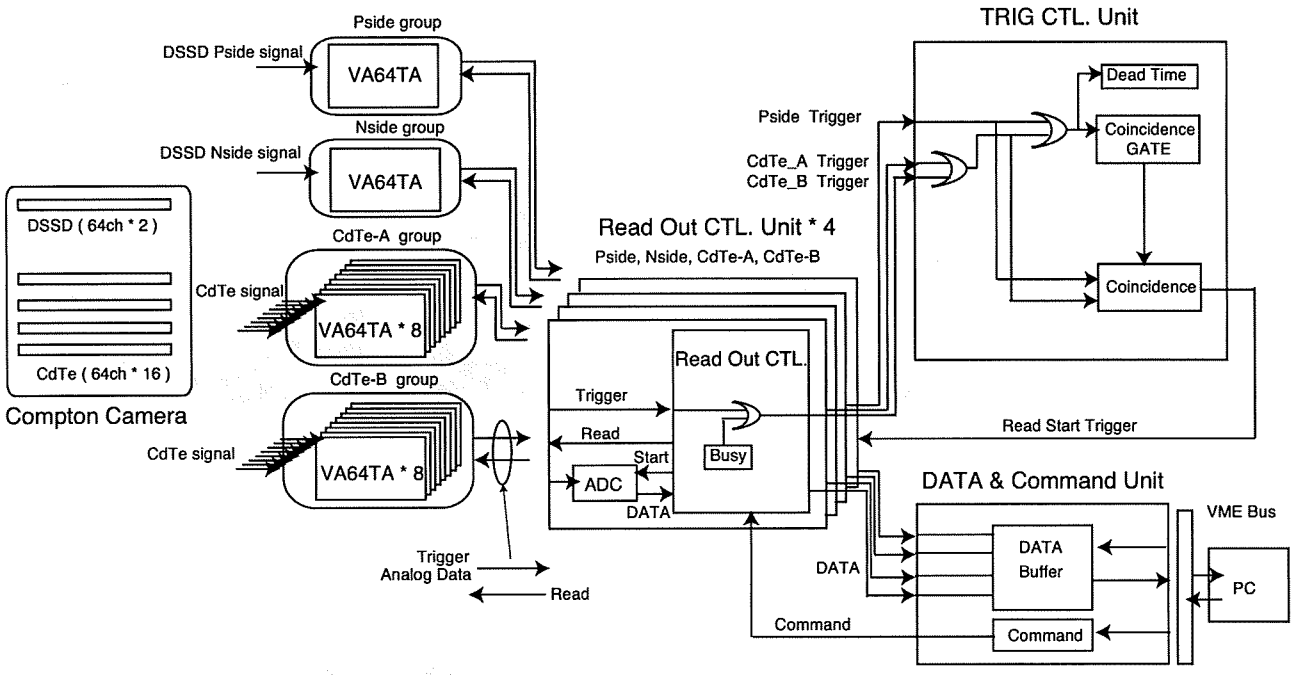

Fig. 6. Schematic diagram of the readout system.

III. Compton Camera Setup

A. Double-Sided Silicon Strip Detector (DSSD)

As a scattering part of the Compton camera, we developed a low-noise double-sided silicon strip detector (DSSD) [9]–[12]. Fig. 3 shows a photograph of the DSSD board. It consists of one DSSD and two low-noise, low-power consumption analog VLSIs (VA64TA1s [13] developed in collaboration with Gamma-Medica Ideas) and mounted on a small circuit board. The DSSD used here is a 2.56-cm wide and 500-μm thick device developed in conjunction with Hamamatsu Photonics, Japan. The strip pitch is 400 μm with a strip gap of 100 μm on each side. The N-side has a floating p-implantation between the strips to isolate the adjacent strips. The Al electrodes are directly coupled on each strip with ohmic contact.

In order to extend the imaging band down to low-energy gamma-rays, low-noise read-out to achieve a lower detection threshold is needed on both the P-side and N-side strips of the DSSD. This is because we need both the P-side and N-side signals to obtain two-dimensional positional information. Thus, a DC-coupled readout is employed for both sides. To apply a reverse bias, the N-side circuit board is biased as a whole. The applied bias voltage is 250 V. The decoupling is held on the digital interface after the analog signal is digitalized by the ADC. The energy resolution at 59.5 keV is found to be 1.6 keV (FWHM) for the P-side and 2.8 keV for the N-side. From the noise level measured on the N-side, we calculated the possibility of incorrectly identifying the position due to random noise, and found that it is less than 10% for a 5 keV energy deposit for this device.

B. 4-Layer Stacked CdTe Module

The absorber consists of a total 16 CdTe pad detectors based on the technology of a high-resolution CdTe Schottky diode [14]–[16]. The production and pixelation of CdTe were performed by ACRORAD, Japan. Each detector is 13.2-mm wide and 500-μm thick. In the CdTe detector, a common electrode made of Indium (In) is used as the anode, and pixelated electrodes divided into 64 pads made of Platinum (Pt) are used as the cathode. The size of each pad of the cathode electrode is 1.35 mm^2, with a gap of 50 μm between the electrodes. A guard-ring electrode surrounds the pads. Due to a high Schottky barrier and the guard-ring electrode, leakage current as low as 10 pA per pad is obtained under bias voltage of 700 V. Good energy resolution is realized thanks to the higher efficiency of charge collection.

Fig. 4 shows the 4-layer stacked CdTe module with a stack pitch of 2 mm [16]. One layer consists of four CdTe pad detectors configured in 2 × 2 geometry and two FECs (Front End Cards) on which four VA64TA1s are mounted. Energy resolution of 2.0 keV (FWHM) is achieved at 81 keV and that of $\Delta E/E \sim 1\%$ (FWHM) is at 511 keV under temperature of $-20°C$, and bias voltage of 600 V. Under these conditions, no significant degradation in spectrum performance was observed during continuous operation of up to two weeks.

C. Setup of the Compton Camera

We constructed the new Compton camera (shown in Fig. 1) by combining the DSSD and 4-layer stacked CdTe module. Fig. 5 shows a cross-sectional view of the camera. The 4-layer stacked CdTe module is arranged 14.7 mm underneath the DSSD. The minimum distance to the target (d_{min}) is 25 mm due to the entrance window provided for thermal decoupling.

Fig. 6 shows a schematic diagram of the readout system. The readout VA64TA1s are divided into four groups: DSSD Pside, DSSD Nside, CdTe-A, and CdTe-B. In the CdTe-A and CdTe-B groups, the eight VA64TA1s are arranged in a daisy chain configuration. The readout sequence of each group is controlled by

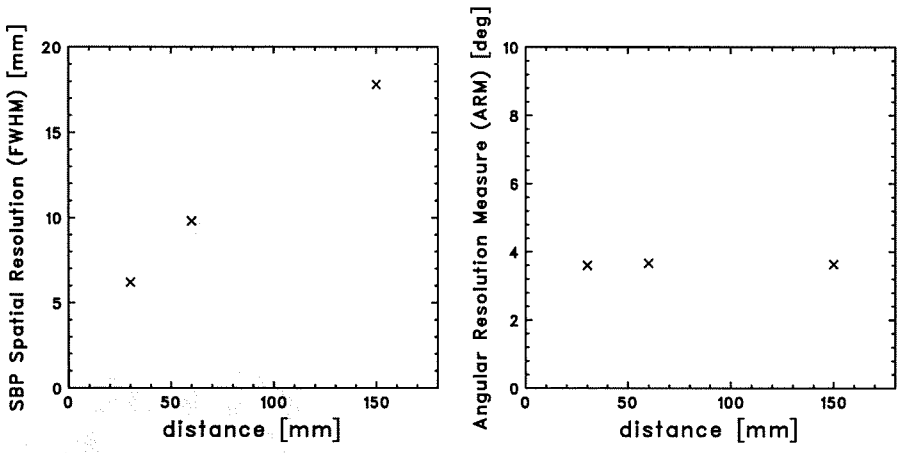

Fig. 7. Left panel showing the distance dependence of spatial resolution of the SBP image; right panel showing that of angular resolution defined by FWHM of the ARM distribution for a 356 keV gamma-ray.

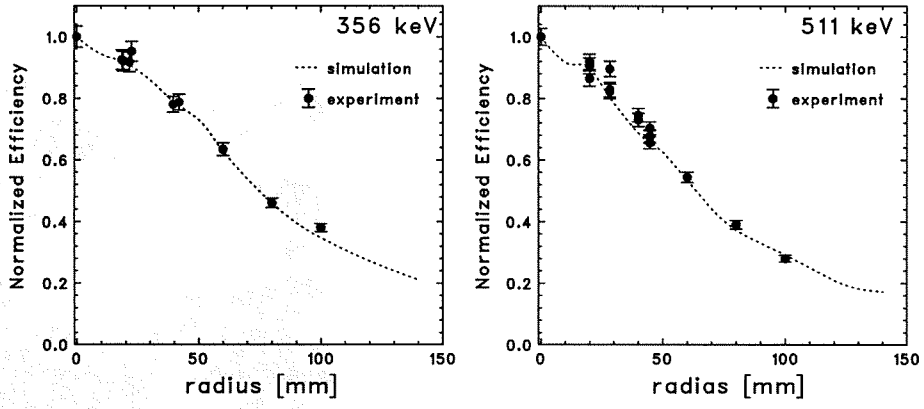

Fig. 8. The position dependence of detection efficiency for 356 keV and 511 keV at d = 60 mm plane. The efficiency at the center position (x, y, z) = (0, 0, 60) in Fig. 5 is set to 1. The radius denotes the distance from (x, y) = (0, 0). The radius 100 mm corresponds to a 120° field of view.

a dedicated Read Out CTL Unit (ROU). The ROU starts the readout sequence by using an external read start trigger. The event trigger from the Compton camera is fed to the TRIG CTL Unit (TCU) that consists of NIM modules in this version. In the TCU, a coincidence judgment is made between the trigger of DSSD and that of CdTe for the effective acquisition of data on Compton events. The coincidence judgment output is then returned to the ROU as a read start trigger. Since this trigger is sent to all ROUs, the pulse heights of all channels are acquired for a coincidence event. The pulse heights converted into digital data in the ROU are then sent to DATA&Command Unit controlled by a PC via the VME bus.

IV. Procedure for Compton Imaging

Data reduction and image reconstruction are performed for Compton imaging. First we select "two hit events", meaning one hit in a DSSD and one in a CdTe detector. Here, the energy threshold to determine a hit is set to 10 keV for both the DSSD and CdTe detectors. Obtaining the Compton events of incident gamma-rays entails the selection of "two hit events" as follows:

- The sum of energy deposits in Si (E_{dssd}) and CdTe (E_{cdte}) is equal to the incident gamma-ray energy (E_{in}), that is, $E_{dssd}+E_{cdte} = E_{in}$. By considering the energy resolution of the detectors, the events where $E_{dssd}+E_{cdte}$ equal $E_{in}\pm$ 5 keV are selected.
- The events where E_{dssd} is from 20 keV to 35 keV are excluded. This region is contaminated by fluorescence X-ray events, which are X-rays from Cd (K_α: 23.1 keV, K_β: 26.1 keV) and Te (K_α: 27.4 keV, K_β: 31.0 keV) escaping from the CdTe detectors and then absorbed in the DSSD.

With these selected events, the Simple Back Projection (SBP) image was obtained. We assumed that incident gamma-rays are scattered in the DSSD and absorbed in the CdTe detector. Based on this assumption, the direction of incident photons is calculated as;

$$\cos\theta = 1 - m_e c^2 \left(\frac{1}{E_{cdte}} - \frac{1}{E_{dssd} + E_{cdte}} \right). \quad (1)$$

The back projection of the Compton cone into the RI source plane is performed event by event. The SBP image is the simple accumulation of Compton cones over all events. The overlapping position of the Compton cones is the origin of the gamma-rays.

Conversely, in the SBP image, most parts of a cone not overlapping with a source become the background. Imaging capability should be improved using a deconvolution method that properly accounts for the response of the Compton camera. We selected a deconvolution algorithm called List-Mode Expectation-Maximizing Maximum Likelihood (LM-EM-ML). Briefly,

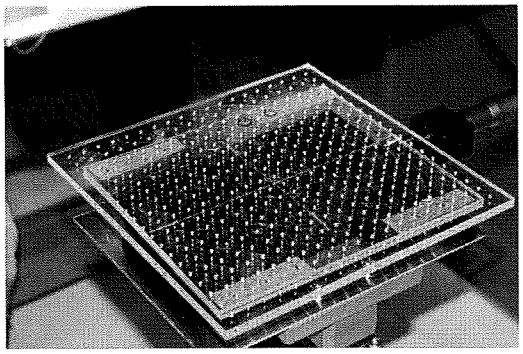

Fig. 9. Acrylic plate with 2 mm diameter holes arranged regularly. The liquid ^{131}I (364 keV) sources were mounted at 20-mm pitch.

this is an iteration algorithm between image space and data space.

$$\lambda_j^{l+1} = \frac{\lambda_j^l}{s_j} \sum_i \frac{t_{ij}}{\sum_k t_{ik} \lambda_k^l} \tag{2}$$

where, λ_j^l denotes the image-bin content at iteration level l, s_j the probability that an event emitted from j is measured, and t_{ij} the probability that a photon emitted from j is measured with the parameters of event i (response). From image space, estimated data space is calculated with a response matrix derived from list-mode data. By comparing the expected data and measured data, corrections are made to image space. A detailed description of the LM-EM-ML method is given in [17], [18].

V. Results

A. Distance Dependence

As mentioned in Section II, the spatial resolution is a function of the distance between the scatterer and target. To demonstrate this concept, we obtained point source data in three cases of $d = 30$ mm, 60 mm and 150 mm. Here, d denotes the distance between the DSSD and the point source, as shown in Fig. 5. The 356 keV gamma-ray source is placed on the Z-axis penetrating the center of the DSSD.

The left panel in Fig. 7 shows the distance dependence of spatial resolution of the SBP image; the right panel shows that of the angular resolution defined by FWHM of the ARM distribution. We evaluated the spatial resolution as FWHM of the SBP image by fitting using a two-dimensional Voigt function. The function is a convolution of Gaussian and Lorentzian distribution, and offers good approximation of a point spread function. We also determined the angular resolution as the ARM distribution in FWHM, by using a one-dimensional Voigt function. The obtained angular resolution was 3.6° and independent of the distance. The spatial resolution (proportional to distance) was about 6 mm and 18 mm at $d = 30$ mm and $d = 150$ mm, respectively. This relation is consistent with the description given in Section II.

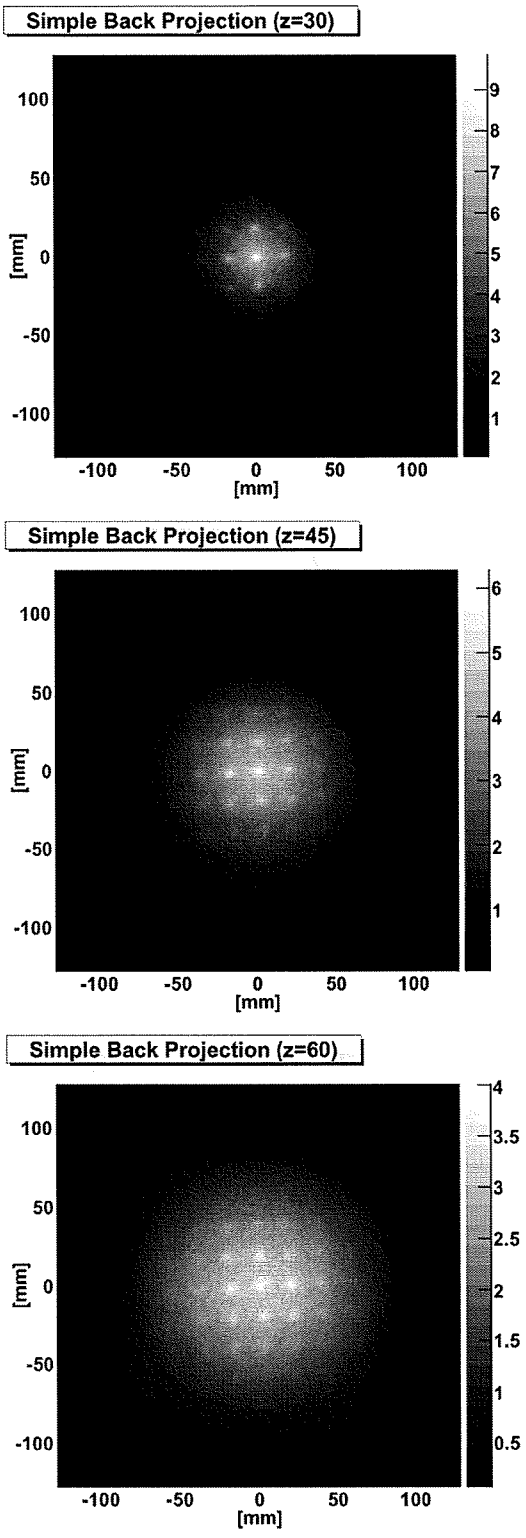

Fig. 10. SBP image of the grid sources in case of $d = 30$ (top), 45 (center) and 60 (bottom) mm. The liquid ^{131}I (364 keV) sources were mounted with a pitch of 20 mm.

B. Field of View

One feature of Compton imaging is a wide field of view. By using 356 keV and 511 keV gamma-ray point sources, we investigated the position dependence relative to detection efficiency. The point source was placed on the plane of $d = 60$ mm (see Fig. 5), and measurements were performed for several positions on the plane. The detection efficiency for each position is obtained from the counts of events where the total energy deposit

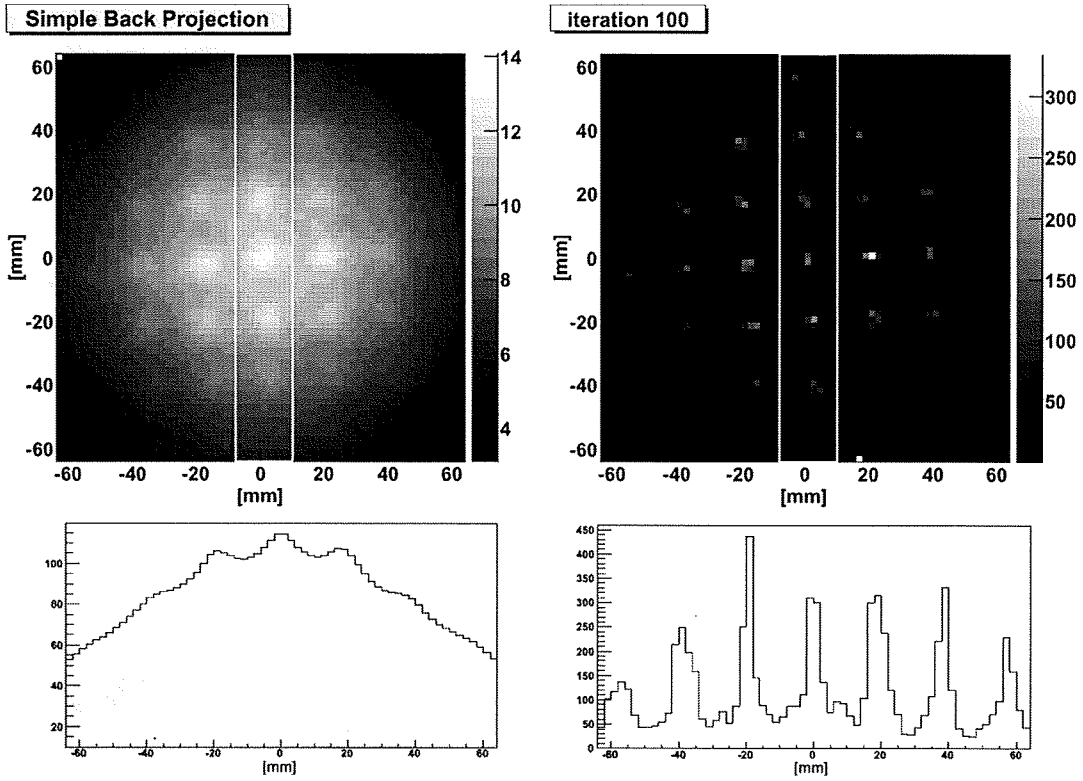

Fig. 11. Deconvolution results for experimental data (d = 60 mm in Fig. 10). The left panel shows the SBP image; the right panel shows the deconvolved image after the 100th iteration. The bottom panel is the projection of the rectangular region of each image to the Y-axis.

$(E_{DSSD} + E_{CdTe})$ is within 356 keV ± 5 keV or 511 keV ± 5 keV.

Fig. 8 shows the position dependence of detection efficiency normalized at the center position of $(x, y, z) = (0, 0, 60)$ for the 356 keV (left) and the 511 keV (right) gamma-rays. The radius denotes the distance from $(x, y) = (0, 0)$. The normalized efficiency at a radius of 100 mm (corresponding to a 120° field of view) is 40% for 356 keV and 30% for 511 keV.

For a detailed evaluation of detection efficiency, we developed a simulator [19] based on the Geant4 toolkit. In the simulation, we included the G4LECS [20] extension in order to estimate the effect of Doppler broadening. The mass model is constructed not only with the detector material, but also with various passive support structures. The energy and position resolutions of the detectors are parameterized based on the experimental results. Fig. 8 shows the normalized efficiency calculated by the simulator, together with the experimental data. The simulation reproduced the experimental results very well. The absolute efficiency derived from the simulator is on the order of 10^{-2}% at the center position for 356 keV gamma-rays.

C. Imaging of Grid Sources

To investigate the resolving power and accuracy of positional determination, an imaging test was conducted using an acrylic plate with 2 mm diameter holes arranged regularly (Fig. 9). The liquid ^{131}I (364 keV, 85 kBq/hole) sources were mounted at 20-mm pitch. The variability of strength of each source is less than 10%. Imaging is performed in three cases: $d = 30$, 45 and 60 mm.

Fig. 10 summarizes the SBP images. The point sources were clearly resolved. The outside sources become visible as d increases, since the sources enter the field of view. Resolving power better than 20 mm was demonstrated up to a distance of $d = 60$ mm, and larger than an 80° field of view as well.

We performed image deconvolution by using the LM-EM-ML method. A total of 1×10^5 events are utilized in this process. A correction factor (s_j) in (2) is derived from the position dependence of detection efficiency calculated by the simulator mentioned in Section V-B. Fig. 11 shows the deconvolution results for the experimental data obtained at $d = 60$ mm. The left panel shows the SBP image; the right panel shows the deconvolved image after the 100th iteration. In the deconvolved image, the point sources placed at the edge become apparent, while only sources located around the central region are resolvable in the SBP image. The bottom panel is the projection of the rectangular region shown in each image to the Y-axis in Fig. 11. Following deconvolution, the peak area of each source becomes stable, thanks to the deconvolution technique that included the correction of efficiency.

It is also important to study the accuracy of positional determination. Therefore, we first derived the center position of the sources from the deconvolved image shown in the right panel in Fig. 11. For the 25 sources arranged in 5×5, the center position of each source was determined by calculating the weighted center around the largest pixel. The center positions are plotted as shown Fig. 12 with open squares. Then based on the assumption that the sources are at the intersection of cross lines at a right angle, we fit the center positions. The red grid in Fig. 12 shows the fitting results. The bottom panel of Fig. 12 summarizes the

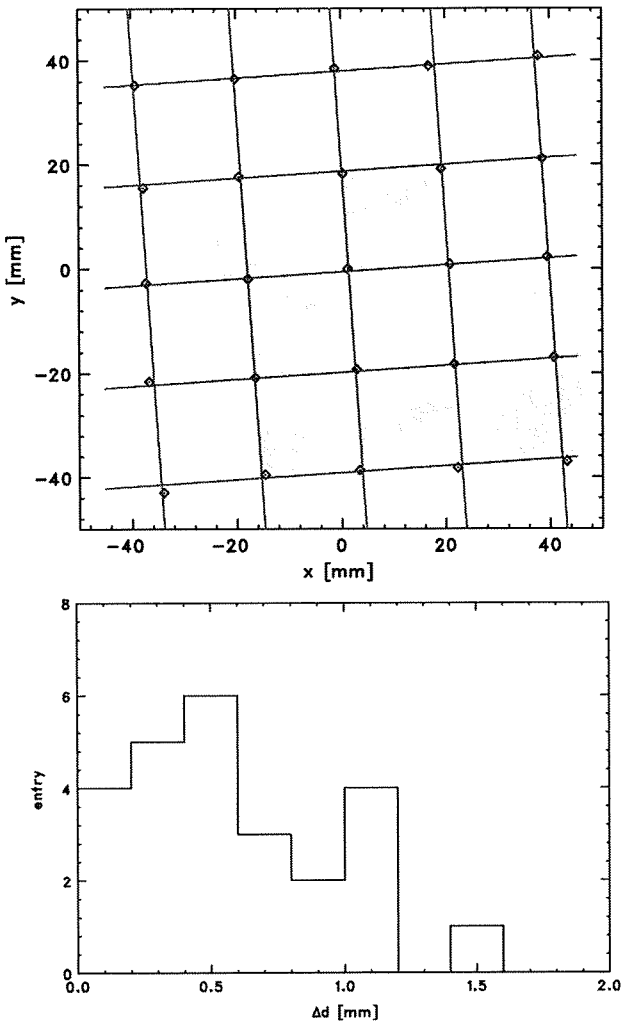

Fig. 12. Top: measurement values of source positions (open square) derived from the deconvolved image shown in the right panel of Fig. 11 in the grid (cross lines). Bottom: distribution of the difference of all 25 sources.

differences of these positions of all 25 sources as distributed within ~1 mm. Thus, this experiment demonstrates positional determination accuracy of 1 mm for the point source.

D. Extended Object

Since the ability to image extended object is a key requirement for both astrophysical and medical applications, we prepared an extended target as shown in Fig. 13. The liquid ^{131}I source (364 keV, 1.6 MBq) is soaked in paper and shaped like an inverted "C" with a gap of 3 mm. The target was placed on the $d = 30$ mm plane.

Fig. 14 shows the images obtained. The top panel shows the SBP image; the bottom panel shows the 10th iteration using the LM-EM-ML method. The shape with a gap of 3 mm is recognized even in the SBP image. With the LM-EM-ML method, the shape is successfully deconvolved. Thus, resolving power better than 3 mm is demonstrated experimentally.

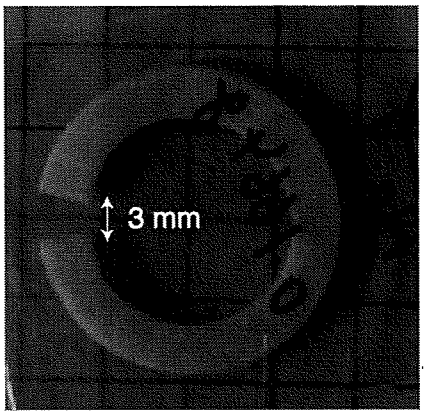

Fig. 13. Photograph of the extended target. The liquid ^{131}I source in soaked in paper, and shaped like an inverted "C" with a gap of 3 mm.

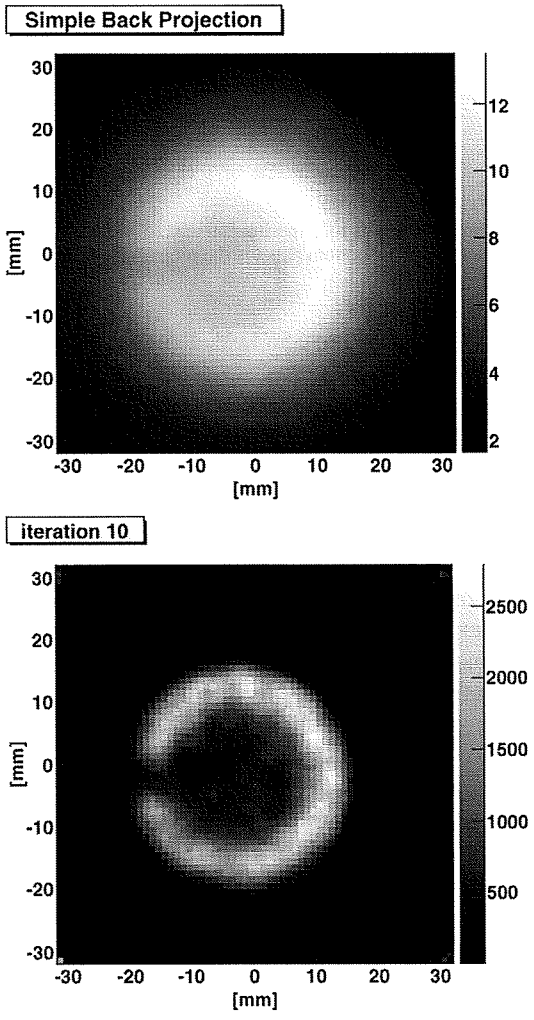

Fig. 14. Results of extended target imaging. The distance to the target is d = 30 mm. The top panel shows the SBP image; the bottom panel shows the deconvolved image after the 10th iteration.

VI. Conclusion

By combining the DSSD and a 4-layer stacked CdTe module, we developed a new Compton camera designed to achieve high spatial resolution. As explained in Section II, the spatial resolution gradually deteriorates as the distance increases between the target and scatterer. Therefore, the camera is designed to

minimize this distance. A minimum distance of 25 mm was realized. Studies were conducted on the field of view, spatial resolution, the accuracy of positional determination, and resolving power. Using the experimental data, resolving power better than 3 mm was demonstrated for a 364 keV (^{131}I) gamma-ray placed 30 mm away from the sensor. Positional determination accuracy of 1 mm was also demonstrated experimentally. Furthermore, the imaging of an extended object was also successfully performed.

As the deconvolution method, we selected an iteration algorithm called List-Mode Expectation-Maximizing Maximum Likelihood (LM-EM-ML). It was applied to several kinds of experimental data. The Compton back projection images derived from the arranged point sources and the extended object were successfully deconvolved.

The results of this imaging test suggest that the Si/CdTe Compton camera is an attractive detector not only for astrophysics application, but also for medical imaging. The data obtained by the experiments also proved effective in investigating the detailed response of a Compton camera used in astrophysics.

REFERENCES

[1] R. W. Todd *et al.*, "A proposed γ camera," *Nature*, vol. 251, pp. 132–134, 1974.

[2] M. Singh *et al.*, "An electronically collimated gamma camera for single photon emission computed tomography," *Med. Phys.*, vol. 10, no. 4, pp. 428–435, 1983.

[3] T. Takahashi *et al.*, "High resolution CdTe detectors for the next generation multi-Compton gamma-ray telescope," in *Proc. SPIE-Int. Soc. Opt. Eng.*, 2003, vol. 4851, pp. 1228–1235.

[4] T. Mitani *et al.*, "A prototype Si/CdTe compton camera and the polarization measurement," *IEEE Trans. Nucl. Sci.*, vol. 51, no. 5, pp. 2432–2437, 2004.

[5] T. Tanaka *et al.*, ""Recent results from a Si/CdTe semiconductor Compton telescope," *Nucl. Instr. and Meth. A.*, vol. 568, pp. 375–381, 2006.

[6] S. Watanabe *et al.*, "A Si/CdTe semiconductor Compton camera," *IEEE Trans. Nucl. Sci.*, vol. 52, no. 5, pp. 2045–2051, 2005.

[7] A. Zoglauer *et al.*, "Doppler broadening as a lower limit to the angular resolution of next generation compton telescope," in *Proc. SPIE-Int. Soc. Opt. Eng.*, 2003, vol. 4851, pp. 1302–1309.

[8] S. Takeda *et al.*, "A new Si/CdTe semiconductor Compton camera developed for high-angular resolution," in *Proc. SPIE*, vol. 6706, p. 67060S.

[9] S. Takeda *et al.*, "Double-sided silicon strip detector for x-ray imaging," SPIE Newsroom [Online]. Available: http://www.spie.org/x20060.xml 2008

[10] K. Nakazawa *et al.*, "A high-energy resolution 4 cm-wide double- sided silicon strip detector," *Nucl. Instr. and Meth. A.*, vol. 573, p. 44, 2007.

[11] H. Tajima *et al.*, "Low noise double-sided silicon strip detector for multiple-Compton gammaray telescope," in *Proc. SPIE-Int. Soc. Opt. Eng.*, 2003, vol. 4851, pp. 875–884.

[12] S. Takeda *et al.*, "Development of double-sided silicon strip detectors (DSSD) for a Compton telescope," *Nucl. Instr. Meth., A.*, vol. 579/2, pp. 859–865, 2007.

[13] T. Tanaka *et al.*, "Recent results from a Si/CdTe semiconductor Compton telescope," *Nucl. Instr. Meth., A.*, vol. 568, pp. 375–381, 2006.

[14] T. Takahash *et al.*, "High resolution Schottky CdTe diodes," *IEEE Trans. Nucl. Sci.*, vol. 49, no. 3, pp. 1297–1303, 2002.

[15] K. Nakazawa *et al.*, "improvement of the cdte Diode Detectors using a Guard-ring Electrode," *IEEE Trans. Nucl. Sci.*, vol. NS-51, no. 4, p. 1881, 2004.

[16] S. Watanabe *et al.*, "Development of semiconductor imaging detectors for a Si/CdTe Compton camera," *Nucl. Instr. Meth., A.*, vol. 579/2, pp. 871–877, 2007.

[17] S. Wilderman *et al.*, "List-mode maximum likelihood reconstruction of Compton scatter camera images in nuclear medicine," in *IEEE Nucl. Sci. Sympo.*, 1998, vol. 3, pp. 1716–1720.

[18] A. Zoglauer, "First light for the next generation of Compton and Pair telescope," PhD thesis, Technische Universitat Munchen, , 2005.

[19] H. Odaka *et al.*, "Performance study of Si/CdTe semiconductor Compton telescopes with Monte Carlo simulation," *Nucl. Instr. Meth., A.*, vol. 579/2, pp. 878–885, 2007.

[20] G4LECS [Online]. Available: http://www.public.lanl.gov/mkippen/actsim/g4lecs/

PHYSICAL REVIEW C 79, 034313 (2009)

Search for a "3.5-eV isomer" in ^{229}Th in a hollow-cathode electric discharge

T. T. Inamura and H. Haba
RIKEN Nishina Center, Wako, Saitama 351-0198, Japan
(Received 29 July 2008; published 18 March 2009)

A hollow-cathode electric discharge, a well-established source in optical spectroscopy, was used to populate the "3.5-eV isomer" in ^{229}Th with use of nuclear excitation by electron transition (NEET). The radiochemically purest ^{229}Th sample was loaded into the hollow cathode in which the electric discharge excited the ^{229}Th to atomic states some of which could be expected to lie close to the excitation energy of the sought isomer. Although there remain some uncertainties, our experiments indicate that the isomer was populated by NEET and its α decay observed after switching off the electric discharge with a corresponding isomer half-life 1 min $\lesssim T^m_{1/2} \lesssim$ 3 min. From the present NEET condition, the isomer appears to lie between 3 eV and 7 eV. The probability of the isomer population by NEET is discussed.

DOI: 10.1103/PhysRevC.79.034313 PACS number(s): 21.10.Tg, 23.20.Nx, 23.60.+e, 27.90.+b

I. INTRODUCTION

Because of its uniquely low excitation in the nucleus, the isomer ^{229}Th^m is important in its own right and in understanding its nuclear structure. But its existence has yet to be established in spite of numerous efforts made experimentally and theoretically for the last three decades. We report an experiment that is expected to significantly advance this study of ^{229}Th^m, Nuclear Excitation by Electron Transition (NEET) in a hollow-cathode electric discharge.

The extremely low-lying isomer at an energy of <100 eV in ^{229}Th was first postulated by Kroger and Reich [1] who studied γ rays following the α decay of ^{233}U. Eighteen years later, Helmer and Reich [2] revised that excitation energy to 3.5 ± 1.0 eV. Since then, the claimed isomer has often been called "3.5-eV isomer" in ^{229}Th. Meanwhile, Burke *et al.* [3] suggested the existence of such a low-energy isomer at $\leqslant$5 eV by observing angular distributions of the ^{230}Th$(d, t)^{229}$Th reaction. Their results are, however, not direct evidence to support the existence of such an extremely low-lying nuclear isomer ^{229}Th^m. Later, several attempts were made to obtain direct evidence. Because the excitation energy corresponds to the uv, mostly optical measurements were attempted to detect the possible $M1$ isomeric transition that was expected to ensue from the α decay of ^{233}U [4–7]. None of them was successful.

Recently, two different attempts were made to determine the lifetime of ^{229}Th^m with use of radiochemical techniques designed to avoid the huge background inevitably caused by the parent nucleus ^{233}U. Browne *et al.* [8] searched for the α decay of the isomer to ^{225}Ra using "fresh" ^{229}Th chemically separated from the parent nucleus ^{233}U. They measured the change with time of the 193-keV γ-ray intensity from ^{225}Ra, and concluded that the half-life of the isomer must be either <6 h or >20 d. Mitsugashira *et al.* [9] measured α-decay spectra of the reaction products ^{230}Th$(\gamma, n)^{229}$Th, ^{229}Th^m. They concluded that the half-life of the isomer was 14 ± 3 h. Their measurements, however, were not self-consistent, and neither gave clear evidence for the existence of ^{229}Th^m. More recently, two new measurements were reported by the Mitsugashira's group [10,11]: First, they searched for photons from an atomic process suggested in theoretical studies [12–14] as well as for the $M1$ transition from the isomer after rapid chemistry to separate the parent nuclide ^{233}U; second, search for the α decay of ^{229}Th^m that is expected to be populated by the β^- decay of ^{229}Ac produced by the ^{232}Th$(\gamma, p2n)$ reaction. In the latter, one can assume higher population for the isomer than in the α decay of ^{233}U. Again, convincing results were not obtained. We also note the work of Gangrsky *et al.* [15] in which the isomer was expected to be populated by nuclear deexcitation of ^{229}Th irradiated with bremsstrahlung from a microtron. No trace of the isomer was detected in the time range between 2 min and 10 h.

There are three extensive γ-ray spectroscopic studies of ^{229}Th: Gulda *et al.* [16] and Ruchowska *et al.* [17] used the β^- decay of ^{229}Ac that was obtained from the decay chain of ^{229}Fr produced by a spallation reaction in a ^{232}ThC$_2$ or ^{238}U target; and Barci *et al.* [18] who relied on the α decay of ^{233}U. However, these inferred only indirectly evidence of ^{229}Th^m. Guimaräes-Filho and Helene [19] reexamined the excitation-energy data of Helmer and Reich and other previous γ-ray studies. They deduced a value of 5.5 ± 1.0 eV. In a recent experiment Beck *et al.* [20] measured the excitation energy E^m by studying the ^{229}Th γ rays with use of the NASA x-ray spectrometer (XRS): Their high-resolution result, $E^m = 7.6 \pm 0.5$ eV, is significantly greater than the currently accepted value of 3.5 ± 1.0 eV. Neither value is a direct measurement of the $M1$ isometric transition, but is deduced from γ cascade-crossover combinations which are considered to involve the isomer. The latter value is corroborated by independent measurements with use of Ge detectors [2,16–18]. The discrepancy in the two values is presently not understood.

Theoretical studies of ^{229}Th^m have been made mainly by Karpeshin *et al.* [12,21] and by Tkalya *et al.* [13]. (Earlier related papers are given in their references.) The latter proposed an experiment to populate ^{229}Th^m with use of synchrotron radiation from the Advanced Photon Source at Argonne National Laboratory, but this experiment has not been reported so far. The experiment by Gangrsky *et al.* mentioned above is similar in principle. Karpeshin *et al.* [12] also proposed an experiment to populate the isomer with use of laser excitation. In practice this would require a precise

knowledge of E^m. This also holds for an experimental proposal of Kálman and Bükki [14], who made a critical study of the theoretical work of Karpeshine *et al.* From the experimental viewpoint, however, these may all be moot without direct evidence for the existence of $^{229}Th^m$.

Karpeshin *et al.* [22] proposed an interesting experiment to ascertain the existence of $^{229}Th^m$ by making use of hydrogen-like ^{229}Th and $^{229}Th^m$ at GSI in Darmstadt. The advantage of this proposal is in the fact that $M1$ transitions between hyperfine structure components of this isomer and the ground state would be enhanced by several orders of magnitude compared to ones in normal atomic ^{229}Th. No actual experiment has been reported. A yet different attempt to get direct evidence of this isomer by collinear laser spectroscopy has been reported by Tordoff *et al.* [23].

II. EXPERIMENT

A. Feasibility study

Two feasibility studies of NEET in a hollow-cathode electric discharge were made by Inamura *et al.*, the first, measurement of photons [24], the second, of α particles [25]. We review these briefly.

In a hollow-cathode electric discharge one can observe atomic excited states in neutral atoms and up to the continuum in singly charged ions. A test was carried out on thorium and it was confirmed that all atomic states in natural Th and Th^{1+} up to $\approx$10 eV could be excited. A first critical test was to confirm that after switching off the discharge there is no afterglow from atomic excited states as delayed photons attributable to the "3.5-eV isomer" were sought. Experiments described in Ref. [25] switched to the detection of the α decay of $^{229}Th^m$, taking advantage of its better S/N ratio.

The optical measurement, made with a uv spectrometer, gave an estimate $N \approx 10^{13}$ for the number of atoms per second at a given excited state [24,25]. By assuming a NEET probability $P_{\mathrm{NEET}} \sim 10^{-10}$ [12], the population of $^{229}Th^m$, $N \cdot P_{\mathrm{NEET}}$, was expected to be $\approx 10^3$ atoms/s. Consequently, a total counting rate of α particles from $^{229}Th^m$ was estimated to $\lambda_\alpha N^m \approx 1.3 \times 10^{-3}$ s^{-1}, i.e., 4–5 counts/h [25] for an isomer half-life of 14 h [9] and for the ^{229}Th source excited in the electric discharge continuously for ten hours. Further, we expected a considerable enhancement factor that could reach even the order of 10^{11} [12,25] as explained below. The feasibility of this experiment was thus deemed possible.

The excitation and deexcitation processes of the NEET are shown in Fig. 1. The enhancement factor arises from the fact that this process is repeated continuously in the dc electric discharge during the expected lifetime of the isomer.

B. Hollow-cathode electric discharge tube

The hollow-cathode tube for the present study was described in Ref. [25]. However, without changing its geometry, we made it possible to install inside an ambient light-tight solid-state detector (SSD) (ORTEC B-type Si detector) with 150-mm^2 active area and 300-μm depleted depth to detect α particles as rapidly as possible after switching off the discharge. In the present study we used the hollow-cathode tube with or without the SSD depending on the assumed half-life of the isomer. It is shown in Fig. 2 with the SSD in place. The cathode consists of an aluminum module with a hollow and its base made of copper.

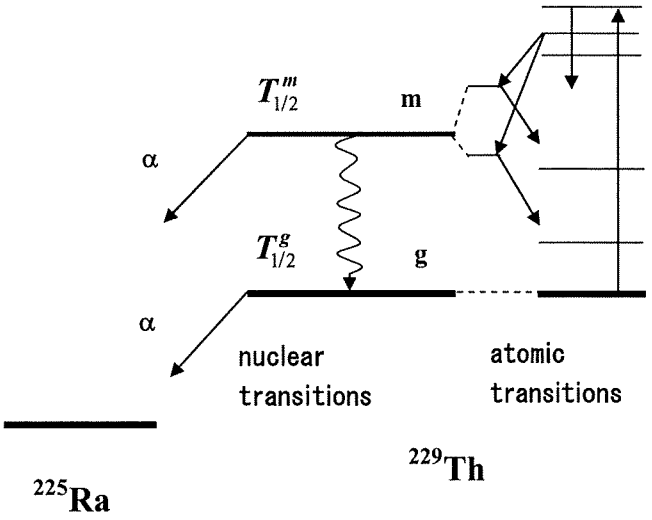

FIG. 1. Schematic excitation and deexcitation processes of $^{229}Th^m$ in the hollow-cathode electric discharge: nuclear ground and isomeric states are denoted by g and m, respectively. Possible intermediate states produced by coupling atomic and nuclear states are denoted by the two short lines.

The thorium sample (as ThO_2—see Sec. II C) is placed inside the hollow from where atoms are sputtered by the discharge-supporting argon gas atoms. The argon pressure was 200 Pa, the discharge current 200 mA dc, and the voltage $\approx$300 V (constant current mode). It is expected that sputtered molecules and atoms are mostly ThO^{1+}, Th, and Th^{1+} [26,27].

C. Source preparation of ^{229}Th

Our ^{229}Th source ($T_{1/2} = 7340$ y) was obtained in May 1980 from the mother ^{233}U sample in a HNO_3 solution by an anion-exchange method. The isotopic impurity ^{232}U in the mother sample was known by α spectroscopy to be 3 ppm. At the beginning, this impurity caused contamination of the separated ^{229}Th by ^{228}Th($T_{1/2} = 1.913$ y), with the ^{228}Th α activity about fifteen times that of ^{229}Th. Today, the ^{228}Th has effectively decayed away to such an extent that it is undetectable. Radiochemically, our ^{229}Th source is almost 100% pure. The ^{229}Th source has been kept in 8 M HNO_3, the concentration of which is 10 mg/L.

Before loading it into the hollow cathode by direct- or electrodeposition, the ^{229}Th source was further purified by the anion-exchange method with use of a chromatographic column (5 mm diameter $\times$40 mm height) filled with an anion-exchange resin (Dowex 1X8, 200–400 mesh): First, 1 mL of the 8 M HNO_3 solution of ^{229}Th was passed through the column to adsorb ^{229}Th by the resin; second, the resin was washed with 4 mL of 8 M HNO_3 to remove impurities such as its daughter elements; and last, the ^{229}Th thus purified was rapidly eluted with pressurized 4 mL 2 M HCl. The resulting elution was

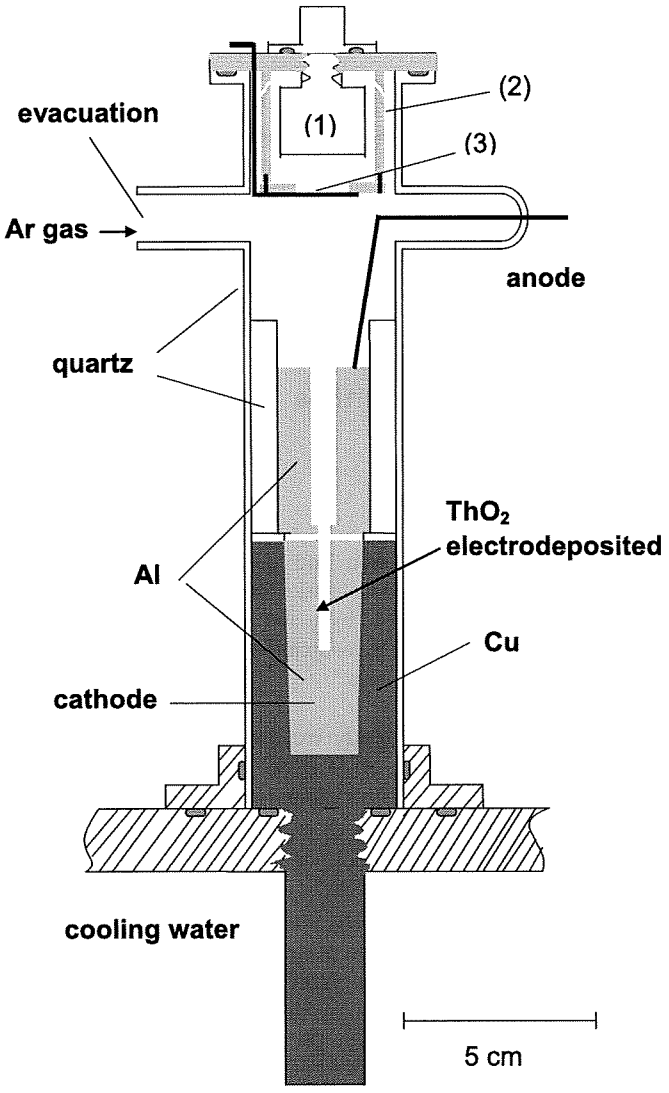

FIG. 2. Cross-sectional view of the hollow-cathode tube with an α-measurement assembly: (1) SSD, (2) aluminum light-shield housing, and (3) a movable shutter to protect the SSD from intense light coming from the hollow-cathode electric discharge. The geometry of the tube is the same as given in Ref. [25].

deposited into the hollow cathode. Alternatively, the elution was dried and then dissolved in 0.5 mL of 0.01 M HNO_3. The concentration of ^{229}Th in the last solution was carefully adjusted by measuring α particles from the ^{229}Th ground state to provide the required source activity.

When the molecular plating method (electrodeposition) [28] was used, a drop (10 μL) of the ^{229}Th in HNO_3 was mixed with 350 μL of 2-propanol to get the appropriate solution. The volume of the hollow, 490 μL, was reduced to $\approx$400 μL after insertion of the 1-mm diameter platinum wire (positive electrode) placed at the center of the hollow and its holder. In this way we obtained the desired uniformly deposited ^{229}Th source inside the hollow cathode, and one in which outgassing is significantly reduced during the discharge.

The electrodeposition was completed in 15 to 30 min. The solution was then washed out with additional 2-propanol and the final efficiency of electrodeposition was found to be greater than 90%.

Before starting the discharge inside the hollow-cathode tube, the aluminum cathode module, loaded directly or by electrodeposition, was baked at 250°C in vacuum for more than two hours. The chemical form of ^{229}Th loaded inside the hollow cathode is considered to be ThO_2 just before the discharge.

D. Measurements

Measurements were made separately in search of ^{229}Th^m depending on its assumed half-life $T^m_{1/2}$.

1. Measurement for $T^m_{1/2} \gtrsim 1$ h

First, we intended to confirm the half-life that Mitsugashira *et al.* [9] reported previously: $T^m_{1/2} = 14 \pm 3$ h. About 1 kBq of ^{229}Th (in a HCl solution as described in Sec. II C) was deposited directly around the middle of the inside wall of the aluminum cathode module. The ^{229}Th source thus prepared was subjected continuously for three hours to the electric discharge in the hollow-cathode tube. After switching off the discharge, the hollow-cathode tube was disassembled rapidly to take out the cathode module and the ^{229}Th source was dissolved with 8 M HNO_3. This solution was passed through the anion-exchange column as described in Sec. II C to purify the thorium source which was supposed to contain ^{229}Th^m populated during the discharge. The thorium elution was co-precipitated with a small amount of samarium as hydroxide with an excess amount of aqueous NH_3. The precipitate filtered on a filter paper (Whatman, Anodisc25) 18 mm in diameter was sintered on the hot plate. This method has proved to provide an excellent α source of ^{229}Th/^{229}Th^m [11].

Twenty minutes after switching off the discharge, we started measurements of α spectra with use of the SSD as a function of time for 17 h. We did not observe significant time-dependent α yields (see Fig. 3). We could not confirm the half-life as was reported by Mitsugashira *et al.* [9]. Next, as described in the following subsection, we tried to make measurements for a short-lived isomer, for which we could adapt our experiment.

Figure 3 shows α spectra observed for the first 10 min, twenty minutes after switching off the discharge and for the last 10 min, seventeen hours after the switching off the discharge. Four clear peaks are from the α decay of the ground state $5/2^+[633]$ of ^{229}Th [29]: the most intense one is mainly of the 4845-keV α transition (56.2), the second is 4901-keV (10.2), the third 4968-keV (6.0) and 4978-keV (3.2), and the fourth 5053-keV (6.6) (the intensities given in the parentheses are percentages of the total α decay of the ground state; the remaining intensities come from α transitions sitting on the low-energy side of the main peak).

2. Measurement for 3 min $\lesssim T^m_{1/2} \lesssim 1$ h

We tried several times to do rapid chemistry in order to shorten the time between starting the measurement and

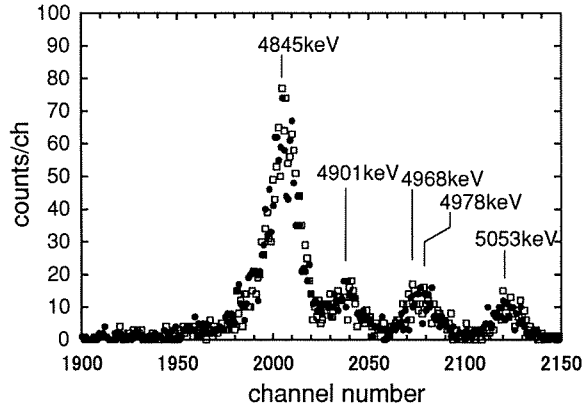

FIG. 3. Comparison of ^{229}Th α spectra recorded each for 10 min, 20 min (•), and 17 h (□) after switching off the dc electric discharge (a period of 3 h) in the hollow-cathode tube loaded with ≈1 kBq of ^{229}Th.

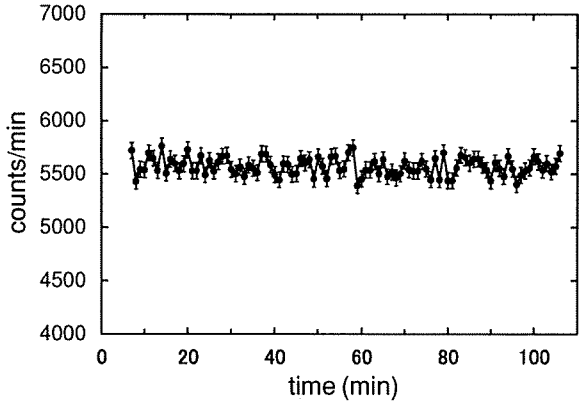

FIG. 5. Total ^{229}Th α yields as a function of time for 100 min, 6 min after switching off the discharge (a period of 30 min). Rapid chemistry was carried out to make the α source.

switching off the discharge, while retaining good energy resolution, 22-keV full width at half maximum (FWHM), for 8376-keV α particles from a daughter nucleus, ^{213}Po, in the decay chain of ^{229}Th. First, 14 min after switching off the discharge, we made measurement of α spectra for 2-min intervals successively for 100 min. Second, 8 min after the discharge, we made the measurement for 5-min intervals successively for 100 min. Finally, we succeeded in making two measurements 6 min after the discharge, and we recorded α spectra for 1-min intervals successively for 100 min. For each measurement the ^{229}Th source was freshly electrodeposited inside a fresh aluminum cathode module as described in Sec. II C, and its activity was increased to ≈5 kBq. The discharge period was 1/2 h and the chemical procedure to get the α source was the same as described in the previous subsection.

Figure 4 shows an example of α spectra from the daughters of ^{229}Th as well as from ^{229}Th. It is seen that α particles from ^{229}Th are well separated from those of the daughters. There is no possibility for the α particles from the daughters to affect the energy range of those from ^{229}Th and to produce any spurious delayed component. Figure 5 shows the total ^{229}Th α yields as a function of time observed 6 min after switching off the discharge. Statistical uncertainties are indicated on the data points. The energy spectra recorded are excellent, but presently no time-dependent α yields are apparent. To further shorten the time between switching off the discharge and starting the measurement, we used the hollow-cathode discharge tube with the SSD inside, as described in Sec. II B, and measured α particles directly from the hollow cathode. This enabled us to start the measurement half a minute after switching off the discharge and evacuating the tube.

Figure 6 shows the total ^{229}Th α yields as a function of time thus observed after being subjected to the discharge for one hour: measurements were made at 5-min intervals over a period of 150 min. The data presented in Fig. 6 are the sum of the first two measurements with the same ^{229}Th source. The source activity was increased to ≈25 kBq. Although statistical fluctuations are large for the entire time range, there appears to be a time-dependent component with a short half-life. To

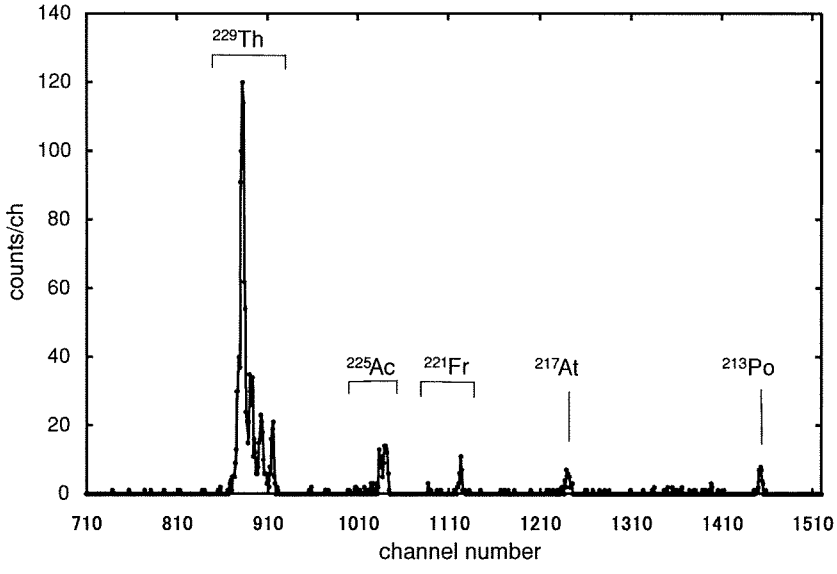

FIG. 4. α spectra from the daughters of ^{229}Th as well as from ^{229}Th observed for 2 min after being subjected to the discharge for 30 min and chemically separated. The activity of the ^{229}Th source was ≈5 kBq.

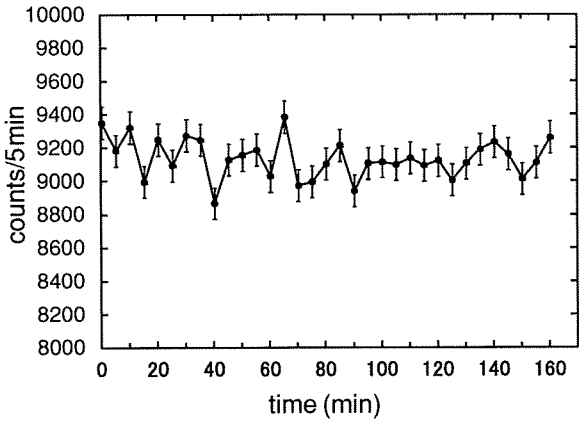

FIG. 6. Total ^{229}Th α yields as a function of time observed inside the hollow-cathode tube after being subjected to the discharge for 1 h. The measurement started half a minute after switching off the discharge and the activity of ^{229}Th source electrodeposited inside the hollow cathode was ≈25 kBq.

check further, we made measurements with 1-min intervals as described in the next subsection.

3. *Measurement for* 0.5 min $\lesssim T^m_{1/2} \lesssim$ 5 min

The ^{229}Th source was electrodeposited and its activity was increased further to ≈40 kBq. Ten measurements were made with this source. The discharge period was 5 min each time. α spectra were recorded with the setup described in Sec. II B half a minute after switching off the discharge and evacuating the tube. Measurements were made at 1-min intervals successively over 30 min for the first three runs and over 15 min for the rest. Figure 7 shows α yields from the ^{229}Th source as a function of time for the ten measurements which were added successively: (a) the total α yields from ^{229}Th and possible ^{229}Th^m; (b) the total daughters' α yields for comparison. The important observation is the decrease with time seen in Fig. 7(a) but not in Fig. 7(b). This trend improves with the better statistics in the first 10 min, as seen in the top data. If we assume that the trend is probably due to the decay of ^{229}Th^m, we will try to extract its half-life as described in the next section.

III. DATA ANALYSIS

To extract the half-life $T^m_{1/2}$ of ^{229}Th^m from the data [top curve in Fig. 7(a)], we have to examine the background level

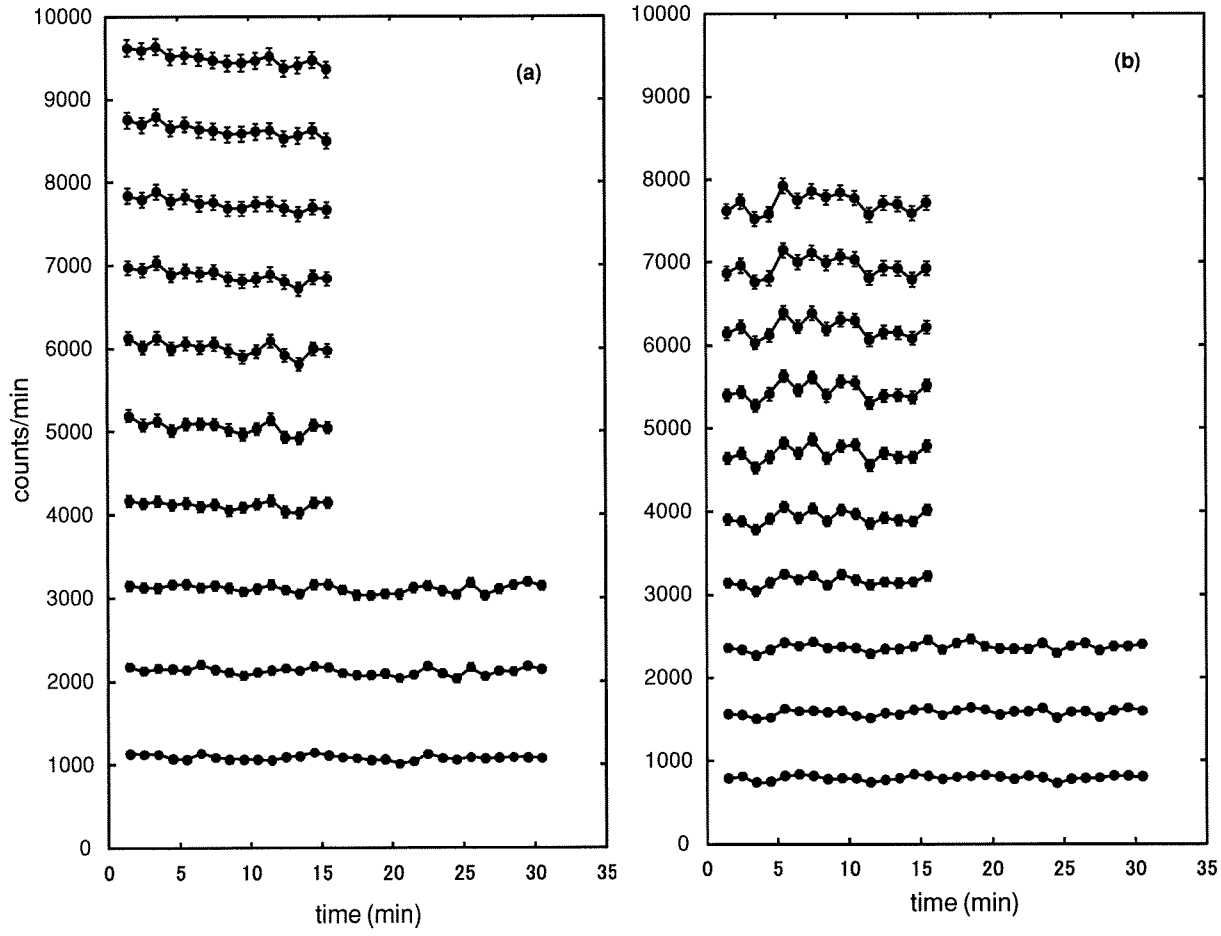

FIG. 7. Total α yields as a function of time for a shorter time range: (a) ^{229}Th and possible ^{229}Th^m; (b) daughters for comparison. The measurement was made as presented in Fig. 6 but with a discharge period of 5 min. The lowest curves are for the first measurement after being subjected to the first discharge. The data were successively added up to the tenth measurement (top curves). The activity of the ^{229}Th source was ≈40 kBq.

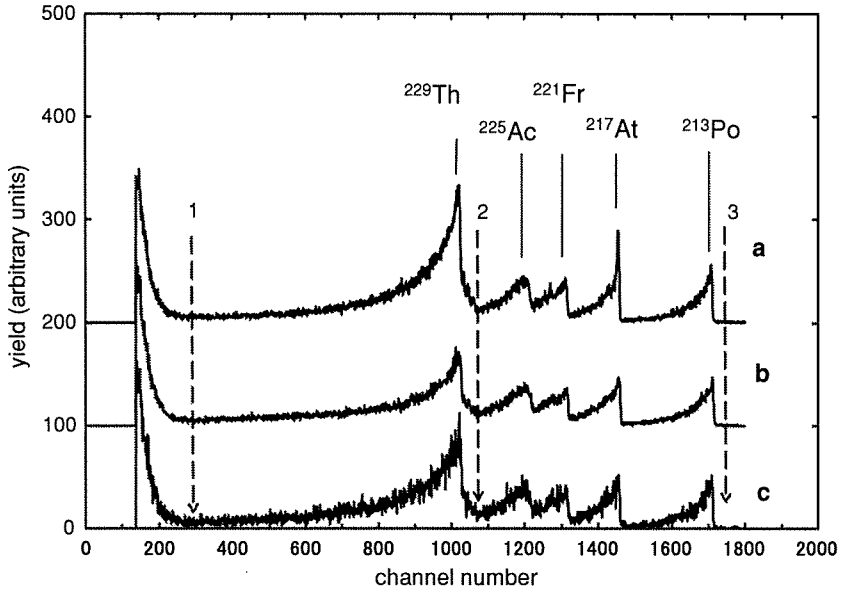

FIG. 8. α spectra observed for 50 min before (a) and after (b) being subjected to the discharge. For comparison, spectrum (c) is presented, which was obtained by integrating measurements over time (0.5–15.5 min) for the first run (see Fig. 7). Spectra (a) and (b) are normalized to 15-min measurements, respectively. Dashed arrow lines 1 and 2 indicate the region of interest to integrate to obtain the total α yields from ^{229}Th and possible ^{229}Th^m as a function of time [see Figs. 6 and 7(a)]. Dashed arrow lines 2 and 3 indicate the α-energy range of daughters which resulted in Fig. 7(b).

due to the α decay of the ^{229}Th ground state. The decay of the ground state ($T^g_{1/2} = 7340$ y) is time-independent in the range of interest. Nevertheless, we have to examine the effects of α emitting daughters, all of which have $E_\alpha > 5100$ keV, because individual α lines might have spread significantly on their lower energy side into the α-energy range of ^{229}Th as a result of the deteriorated energy resolution of α spectra recorded inside the hollow-cathode tube. The ^{229}Th source position was seen obliquely by the SSD (see Fig. 2) and the energy resolution significantly diminished (see Figs. 3, 4, and 8 for comparison).

The α emitting daughters in the decay chain are [29]: ^{225}Ra (14.8 d) $-\beta^-\rightarrow$ ^{225}Ac (10.0 d) $-\alpha\rightarrow$ ^{221}Fr (4.9 min) $-\alpha\rightarrow$ ^{217}At (32.3 ms) $-\alpha\rightarrow$ ^{213}Bi (45.6 min) $-\beta^-\rightarrow$ ^{213}Po (4.2 μs) $-\alpha\rightarrow$ ^{209}Pb (3.25 h) $-\beta^-\rightarrow$ ^{209}Bi. Figure 8 shows a comparison of α spectra observed before and after the discharge in the third measurement (Sec. II D 3). There is no significant difference among the α spectra except for a loss of ^{229}Th caused by sputtering during the discharge. The loss of the ^{229}Th source is significant, but does not affect time-dependence of α yields.

As is seen from Fig. 8, the individual α lines are spread out over the lower energy side and prevented the identification of any weak α transitions attributable to the decay of the isomer. It also means that any possible α transitions from the isomer are definitely less than ten percent of the total α-decay rate of the ^{229}Th ground state (see the known relative intensities of its components given in Sec. II D 1); we note that the three weak α lines from the ground state were in fact observed. While the energy spectra may overlap, we recall Figs. 7(a) and 7(b) that indicate a significant difference as a function of time. Therefore, we conjecture that ^{229}Th^m was populated by NEET during the discharge and it disappears in minutes.

With this conjecture the total counting rate of α particles from ^{229}Th and ^{229}Th^m at time t is written as

$$n_\alpha(t) = \lambda^m_\alpha N^m(t) + \lambda^g_\alpha N^g(t), \tag{1}$$

where λ^m_α is the α-decay constant for ^{229}Th^m, and for the ground state ^{229}Th $\lambda^g_\alpha \equiv \lambda^g = \ln 2/T^g_{1/2}$. We take $t = 0$, the time when the discharge is switched off. At time t, the number of ^{229}Th^m atoms, $N^m(t)$, and the number in the ground state ^{229}Th, $N^g(t)$, are given, respectively, by

$$N^m(t) = N^m(0)e^{-\lambda^m t}, \tag{2}$$

$$\frac{dN^g(t)}{dt} = \lambda^m_p N^m(t) - \lambda^g N^g(t), \tag{3}$$

where λ^m_p is the total photon-decay constant for the isomer. Noting $\lambda^m_p \approx \lambda^m = \ln 2/T^m_{1/2}$ because $\lambda^m_\alpha \ll \lambda^m_p$, we obtain from Eqs. (2) and (3)

$$N^g(t) = N^m(0)\frac{\lambda^m}{\lambda^g - \lambda^m}\left(e^{-\lambda^m t} - e^{-\lambda^g t}\right) + N^g(0)e^{-\lambda^g t}, \tag{4}$$

the number of ^{229}Th atoms before the discharge is given, approximately, by $\overline{N} = N^m(0) + N^g(0)$.

Noting that $T^g_{1/2} = 7340\,y$, and $\lambda^m \gg \lambda^g, t \ll T^g_{1/2}$ or $\lambda^g t \ll 1$, we have from Eq. (4)

$$N^g(t) \approx \overline{N} - N^m(0)e^{-\lambda^m t}. \tag{5}$$

Combining Eqs. (1) and (5), we obtain

$$n_\alpha(t) = \left(\lambda^m_\alpha - \lambda^g\right) N^m(0)e^{-\lambda^m t} + \lambda^g \overline{N}. \tag{6}$$

The second term gives the background, i.e., α particles from the ground state. When we make successive measurements at intervals Δ following a time Δ_0 after switching off the discharge, we can reduce Eq. (6) to

$$n_\alpha(t_i) = Ce^{-\lambda^m t_i} + \lambda^g \overline{N}\Delta, \tag{7}$$

where $t_i = \Delta_0 + i\Delta$, $i = 1, 2, 3, \ldots$ and $C = [(\lambda^m_\alpha - \lambda^g)/\lambda^m]$ $N^m(0)(e^{\lambda^m \Delta} - 1)$. In fact, the second term should also include the environmental background.

In principle, it should be possible to fit the data to a function of the form Eq. (7) in order to extract the isomer decay constant λ^m. Unfortunately, statistical uncertainties are not sufficiently small to allow a linear least-squares fit to the residue after background subtraction on the logarithmic scale. Instead, we examine the decay properties by non-linear least-squares of